



Salt weathering in granitoids: an overview on the controlling factors

Luís Sousa^{1,3} · Siegfried Siegesmund² · Wanja Wedekind²

Received: 31 January 2018 / Accepted: 23 June 2018 / Published online: 3 July 2018
© Springer-Verlag GmbH Germany, part of Springer Nature 2018

Abstract

Historically granite is one of the most applied building materials worldwide. Building stones should accomplish several properties required by different testing materials standards. Salt weathering affects the aesthetical properties of the stones and eventually diminish their durability. The use of weathered granites has increased in the last several decades, but their behavior under adverse environmental conditions requires continued investigation. The use of salt for the prevention of ice formation in colder climates can have harmful consequences on high-porosity stones. Twenty-eight different stones, mostly granitoids, all of them often used as dimensional building stones, were subjected to the salt bursting test. The porosity and the pore network are important parameters in salt weathering; therefore, the pore radii distribution and capillary water uptake were measured. The capillary pores and related porosity are the main factors controlling the behavior of the studied stones under salt action. However, the pore radii size and distribution also plays an important role. In some cases, the salt action is only visible after a high number of test cycles, thus making the actual salt test standards unrealistic.

Keywords Salt weathering · Granite · Pore radii distribution

Introduction

Building stones begin undergoing alterations once they are emplaced for their specific purpose under the prevailing environmental conditions. These can become perceptible in a short time period after placement (Comite 2017). The rate of changes depends on both environmental conditions and rock properties (Viles 2013; Graue et al. 2013; Molina et al. 2015; Abad et al. 2016). In the literature, it is common to find research papers on stone conservation and the weathering of different rock materials such as sandstones (Ruedrich and Siegesmund 2007; Thomachot-Schneider et al. 2008;

Stück et al. 2013; Molina et al. 2015), limestones (Laycock et al. 2008; Espinosa-Marzal et al. 2011; Siegesmund et al. 2010), tuffs (Arıkan et al. 2007; Wedekind et al. 2013; López Doncel et al. 2016) and carbonate stones (Benavente et al. 2004; Unterwurzacher and Mirwald 2008). Studies on the behavior of granites undergoing weathering are not very common, probably because this rock has low porosity and consequently the deterioration is less effective (Vázquez et al. 2013, 2016; Sousa et al. 2017).

Many decay features have been studied and classified. Some of the damages observed on many buildings are flaking, scaling, alveolization, lamination, cracks, efflorescence and subflorescence. Figure 1 presents examples of weathering forms found in granitoids. These and other deterioration forms can be better studied in ICOMOS-ISCS (2008) and Siedel and Siegesmund (2014).

Salt crystallization is a constant in the natural landscape as a geomorphological feature, especially in coastal areas (Cardell et al. 2003) and deserts. Archeological artifacts like ceramic amphoras also exhibit this process of deterioration. However, when it comes to building materials used in ancient buildings and heritage monuments, the whole building architecture can be seriously compromised. Weathering caused by salt crystallization can be considered one of the most aggressive decay forms (Correns and Steinborn 1939;

This article is part of a Topical Collection in Environmental Earth Sciences on “Stone in the Architectural Heritage: from quarry to monuments – environment, exploitation, properties and durability”, guest edited by Siegfried Siegesmund, Luís Sousa, and Rubén Alfonso López-Doncel.

✉ Luís Sousa
lsousa@utad.pt

- ¹ Department of Geology, University of Trás-os-Montes e Alto Douro, Quinta de Prados, 5000-801 Vila Real, Portugal
- ² Geoscience Centre, University Göttingen, Goldschmidtstrasse 3, 37077 Göttingen, Germany
- ³ CEMMPRE Research Centre, Coimbra, Portugal

Fig. 1 Example of weathering forms on granitoids: scaling (a), black crusts (b), pitting (c), oxidation (d), alveolization (e), missing part (f) and graffiti (g)



Doehne 2002; Hosono et al. 2006; Begonha 2009; López-Arce et al. 2011; Steiger et al. 2014). The results of its damage is observable on different materials at different scales, places and times (Liu et al. 2014; Momeni et al. 2017). Therefore, studying salt crystallization and its behavior within the stone it becomes possible to gain a deeper understanding of the behavior of granites undergoing salt burst testing conditions. This will aid in verifying the influence of the pore size distribution, porosity, water vapor diffusion (WVD) and water absorption, so that it can be possible to evaluate if existing heterogeneities could be responsible for the weathering of granite due to salt crystallization. At coastal and desert areas alveolar weathering is often found that can be traced back to the salt in sea- or rain-water that mainly contains chlorides (Fig. 1e). In urban environments, crusts are often formed due to soluble components in air pollution and to the creation of gypsum and other salts that contains sulphates. These crusts create weathering forms like contour scaling (Fig. 1b). At the rural areas weathering

forms as flaking can be traced back to the crystallization of nitrate salts (Fig. 1a).

In a supersaturated solution, the growing crystals exert pressure as verified in the experiments of Correns and Steinborn (1939) and Caruso and Flatt (2012). Supersaturation can be generated by a combination of variations in temperature and concentration: e.g., cooling under constant concentration, concentration increase by evaporation with constant temperature, and changes in both temperature and concentration (Winkler 1973). The pore pressure from crystal growth can cause a lack of cohesion between the grains and is controlled by saturation degree, pore structure and the energy difference between the pore wall and the salt crystal (see Benavente et al. 2004a, b; Steiger et al. 2014). Higher saturation degrees will lead to high crystallization pressure and larger pores will have lower crystallization pressure. High energy is necessary to overcome the electrostatic forces and to develop a direct contact between the salt and the porous material (Steiger et al. 2014). Crystallization begins in the

larger pores and the crystallization pressure is lower. When evaporation of salt-saturated material in solution occurs, it is characterized by two phases, the first phase is liquid and the second is gaseous. In the liquid phase the transport of the solution is faster, being dependent on the pore structures as a function of the forces exerted by the capillarity (Sawdy-Heritage et al. 2008). In the second phase, as the liquid evaporates, first from the macropores, the capillary flow becomes increasingly discontinuous and the transport becomes a vapor phase (Sawdy-Heritage et al. 2008). The crystals grow in the pores and, filling this space, continue to grow against the walls of the pores until the limit of the elastic resistance of the rock is exceeded by the pressure inside the pore, which leads to rock expansion and cracking (Correns and Steinborn 1939; Theoulakis and Moropoulou 1997; Ruedrich and Siegesmund 2007). The crystallization pressures are high enough to cause damage in all the stones (Steiger et al. 2014).

Salts can enter the stone structure as saline solutions associated with moisture (Winkler 1973) and are dragged into the pores by ground capillary uptake, saline spray, rainwater, leaking pipes, gutters and insufficient ventilation (see Steiger et al. 2014). When the solvent evaporates, the crystals formed occupy a larger volume than the previous physical state as salt solution, breaking the cohesion between the grains. Therefore, to understand the behavior of the stone material under salt bursting conditions, it is necessary to have in mind that the salt crystallization effects depends on the presence of water (López Doncel et al. 2016). The available water depends on the environmental moisture and the stone porosity (Steiger et al. 2014). Efflorescence and subflorescence are two mechanisms which leads to salt weathering on stones, bricks and mortars (Flatt et al. 2017). The efflorescence is a visible white patch. It is evidence of salt growth on the surface of a porous material and occurs because the fluid moves during evaporation and migrates to the surface. The efflorescence causes color and roughness changes but normally do not harm the structure (Winkler 1973). The subflorescence results from the crystals growing within the porous stone causing damage like cracks, scaling and granular disintegration (Flatt et al. 2017).

Research on the action of salt in granitoids is still relatively new and not much has been published (Alonso et al. 2008; López-Arce et al. 2010; Vázquez et al. 2008, 2013; Sousa et al. 2017). In granites, the consequence of salt weathering is visible with the naked eye on the stone surface. The detachment of mica from the surface and the existing cracks among quartz and feldspars causes physical damage (Vázquez et al. 2013; Sousa et al. 2017). Evaluating the influence of the factors controlling salt deterioration in a large number of different granitoids has never been systematically done. The present research contributes to this difficult undertaking.

Case of study

One interesting case study concerning the weathering effect of salt crystallization on granites is the Middle Ages tower located near Vila Real in northern of Portugal. The tower is designated a national monument and is known as the Quinta Tower (<http://museu.cm-vilareal.pt/index.php/torre-de-quintela>). Although not much is known about its construction, possibly in the eleventh century, the history of this building goes back to the time of the Christian Reconquest, when the borders of Portugal were being created and the battles against the Moors were coming to an end. This tower has resisted the forces of time, and apparently shows no changes to its original main shape. It was luckily preserved because its last owner sold it to a stonemason for the reuse of its stones. Fortunately, the stonemason could not find a practical way to remove the stone blocks and the building has been preserved until today.

The original structure is made from three different types of granites. These stones occur in several overlying rows sustaining the walls up to 30 m. The foundation has the shape of a square, and from the bottom to the top three floors are visible. The first pavement has one main door but no windows. The second has four very narrow vertical gaps, one on each side, which could be protected windows. The last floor has four balconies, one on each side and follows the same alignment of the previous gaps. The rooftop has four balconies, one on each corner, and two gargoyles, one to the east and the other to the north for drainage of rainwater.

Interesting features of decay are visible with a closer look at the granite walls of this building. The main weathering features observed are fractured surfaces, scaling, back-weathering, biological colonization, color changing, cracks and efflorescence. Black crusts were not observed on this tower, which is a feature that is commonly seen on different monuments, and might be consequence of the rural environment where this monument is located (Fig. 2a). The individual decay features at the tower will be described below.

Scaling due to bursting and chipping

This occurs as detachments on the surface of the granite blocks, especially on the medium-grained granite. Mean size of the scaling range from 0.5 to 8 cm. Visible is the existence of a progressive damage from the limit to the center of the stones blocks.

Efflorescence

This salt growth is commonly visible in the interior of the building. On the exterior, this is sporadically observable due to the washing effect of rain and is associated with the coarser granite type, which is the most weathered one. Only

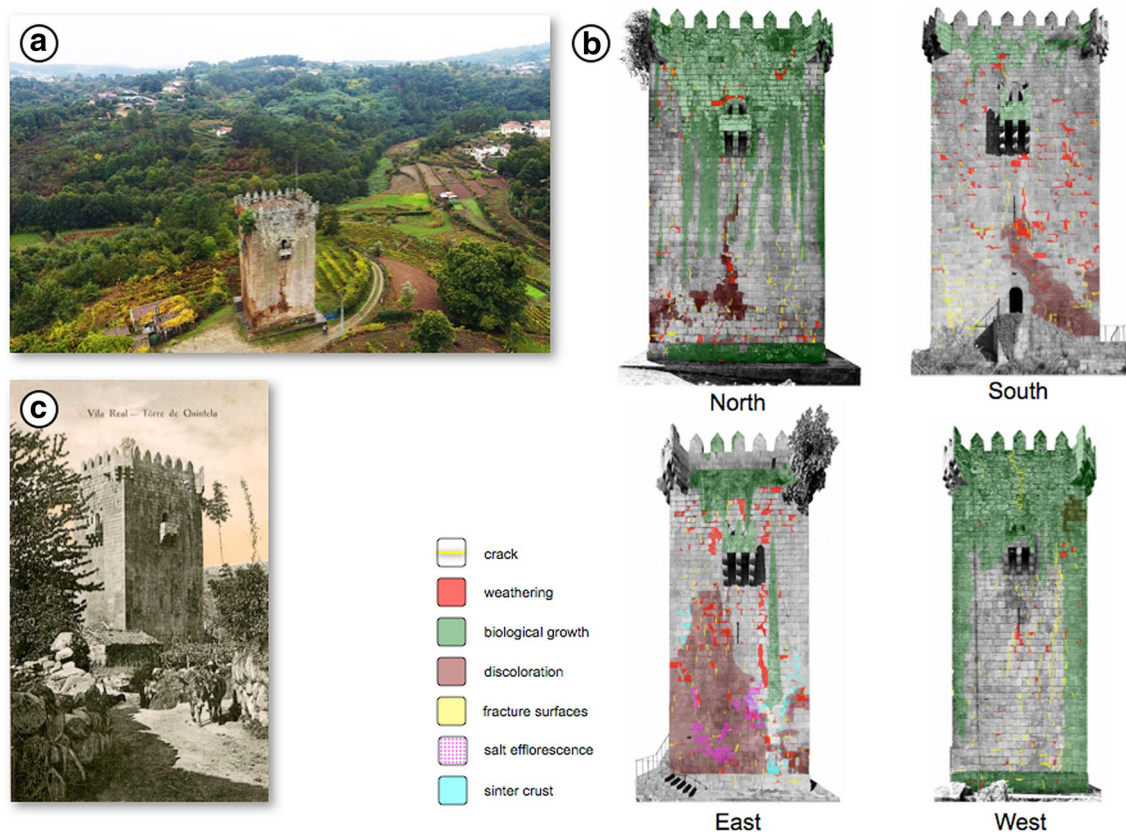


Fig. 2 **a** The Quintela Tower within its environment, **b** decay mapping from the four façades and **c** a historical postcard from around 1900

on the east façade are salt efflorescences found (Figs. 2b, 3a, b).

Cracks and fractures

These are widely observed on all four sides. Cracks can be seen at different locations on the stone blocks and fractures are mostly seen on the edge and have different orientations (Fig. 3e). Some pieces of the corner are even lost. Special attention is given to the west side where most of the cracks can be observed (Fig. 2b). At the same façade a vertical crack goes from the bottom up to the top, with an opening of 2 cm on the bottom. Most of this crack contours the stones along its mortar joints, but also crosscuts some of the stone blocks.

Biological colonization

Different kinds of lichens grow widely over the stone surfaces, with the west façade showing 53% and the north façade exhibiting 32% (Fig. 2b). A major plant (identified as an olive tree) can be seen on the north-eastern edge at top of the tower (Fig. 2). The roots of this tree are also visible in the inside of the tower on the last floor.

Back weathering

This is visible all over the building as a loss of material, especially in the granite with the coarser mineral grains. However, most of the back-weathering effects are observable at the east side (7%), followed by the south side (4%), and the north and west side (around 2%).

Color changing

A brown reddish color is clearly observable on the east side, as well as on the north and south façade (Fig. 2b). It has a greasy aspect and a strong smell of oil derivate material (Fig. 3c). Color changes also occurs as a whitening of a specific area, where the rainwater flows down and washes the stone. Calcite crusts are found at the east side (Fig. 2b).

Each façade also has a predominate weathering form. A clear difference is seen at the east and west facades. The east side shows a high level of cracks, coloring and back-weathering, while the west façade exhibits biological colonization as the main feature.

Using the test pad method in combination with electrical conductivity measurements, detection of the most soluble

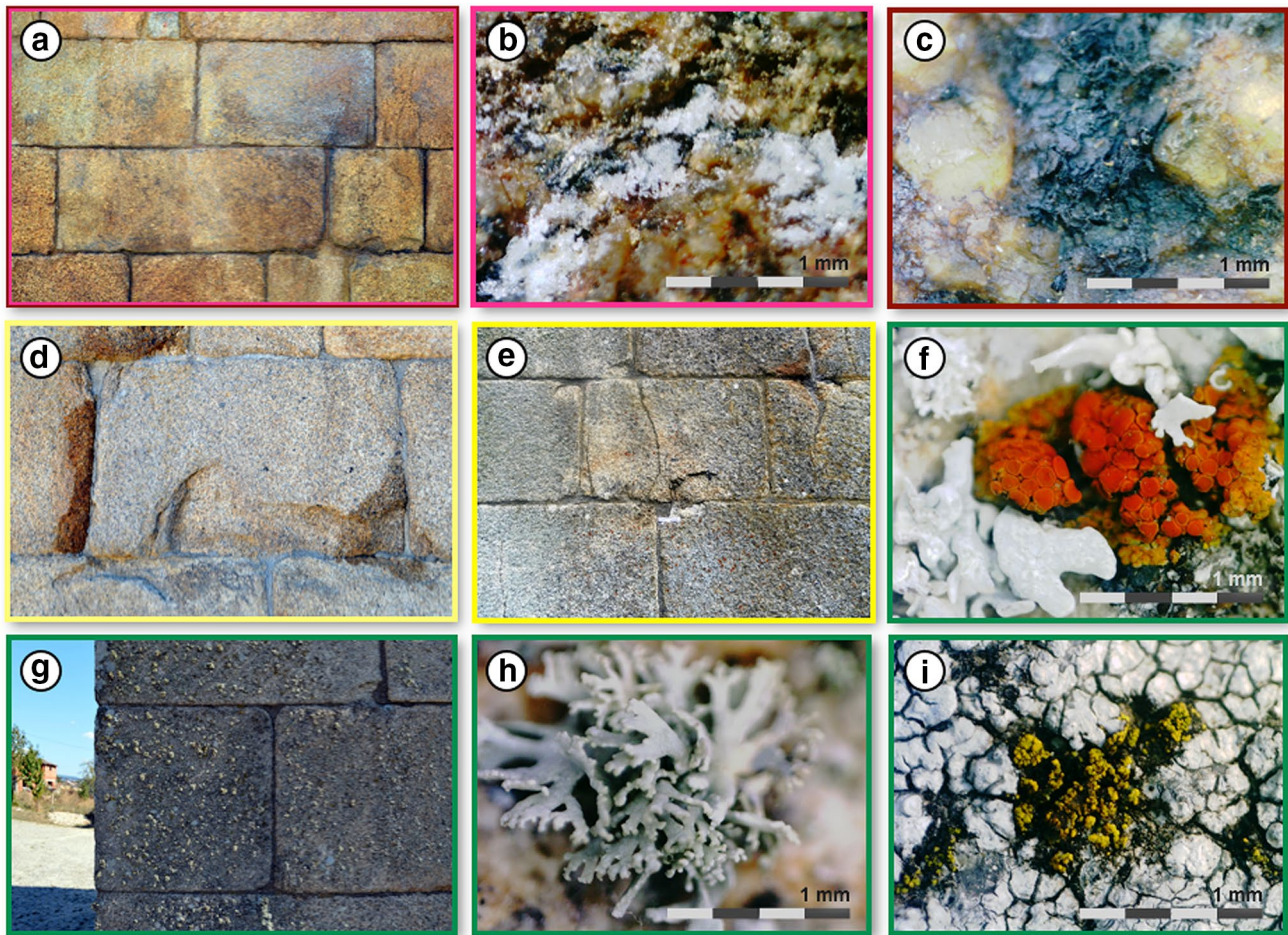


Fig. 3 Observed decay forms and conditions on the Quintela Tower. **a** Salt efflorescence in a macro-scale and **b** in a micro-scale, **c** greasy derivate material that is creating massive discoloration also observable in **a** and **b**, **d** scaling due to bursting and chipping, **e** cracks and fractures as well as partly colorful microbiological growth at the

north site of the tower, **f** reddish and whitish lichens at the north site in a micro scale, **g** bigger whitish lichens are dominating the microbiological growth at the west site of the tower and **i** at the west site also greenish lichens can be found

deposits like salts can be found at the east side of the tower (Fig. 4b). At the northern and southern façade, single ashlar with a high contamination by soluble deposits are concentrated at the areas of discoloration (Figs. 2b, 4b). The west side only shows a few spots of contamination (Fig. 4b).

The identification of the source of salt contamination is still under investigation and the studies on the Quintela Tower are in progress. One possible source for the site-specific salt contamination could be, that parts of the tower were once used as a stable and houses were built against the massive walls of the tower (Fig. 2c).

This example shows that stone decay in monuments has different origins and the salt action is only one of the causes which should be considered. Furthermore, the several factors (mineral composition, water, temperature, etc.) governing the decay process act together and the salt action can be a consequence and cause of other weathering processes.

Materials and Methods

Material

For this study 28 stones (Table 1; Fig. 5) with different characteristics were considered. Samples selected come from Portugal (AR1, BR1, BM1, MB1, MB2, P1, P2, P3, P4 and TQ1), China (TT Black, G603, G654, G682, G603new, G341, Black Singoish and Puerto ALP), Vietnam (V1 and V2), India (Indian Black), Brazil (Verde Bahia and Candéias) and Germany (Flossenburg and Walenstien).

The selected stones show different grain sizes, textures and degrees of weathering. The yellow granites are used often as a building stone (Sousa et al. 2017). It is important to assess their behavior under salt action, and therefore, several yellowish stones were selected for this research. Some metamorphic stones with similar compositions to granitoids

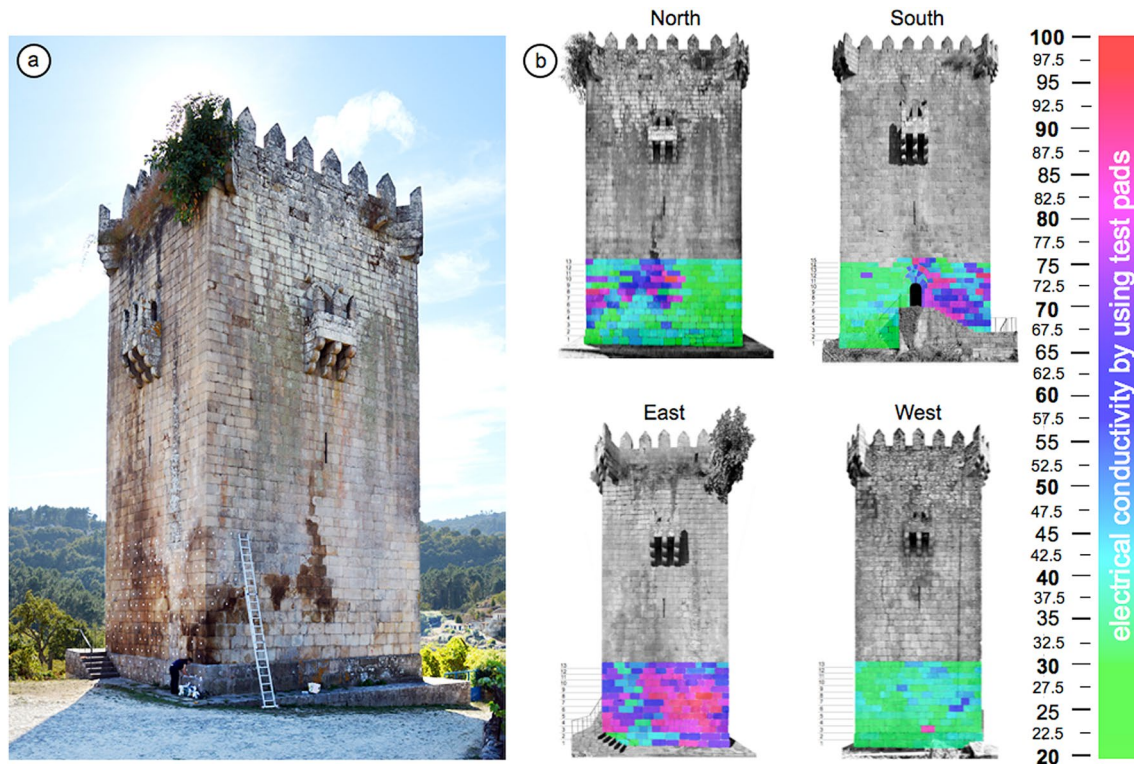


Fig. 4 **a** Performing the test pad method of the first 13 ashlar rows at the tower and **b** the electric conductivity at the different facades of the tower

were also used in this study (e.g., Indian Gold, Paradiso and Viscount-India, all from India).

Methods

The open porosity and density were measured on 5 cm cubic samples using the hydrostatic weighting method (DIN 52102). The water absorption under atmospheric conditions (W_{atm}) and the water absorption under vacuum (W_{vac}) were determined for calculating the saturation coefficient ($W_{\text{atm}}/W_{\text{vac}}$) (see Siegesmund and Dürrast 2014).

The capillary water absorption was measured on cubic samples with dimensions of 6.5 cm in length. The bottom plane of the cubes was placed into water (until a meniscus formed surrounding the entire sample) and the weight increase was measured.

The pore size distribution was measured by mercury intrusion porosimetry (MIP; Pascal 140 and Pascal 440 from Thermo Scientific) using irregular samples (ca. 1.0–1.5 g). Pressures up to 400 MPa were used to evaluate the pore radii measured at around 0.005 μm .

The salt crystallization test was performed according to the standard DIN EN 12370. The samples (5 cm cubes) were soaked in a 10% Na_2SO_4 solution. The samples were submerged for about 4 h in the solution and then dried in an oven

at 60 °C for 16 h. After cooling to room temperature for 4 h, the cubes were weighed to determine the loss of material.

The WVD resistance value was assessed using the wet-cup method on disc-shaped samples (40 mm \times 10 mm). They were placed inside a controlled climate chamber at a temperature of 20 °C and 50% humidity (see Siegesmund and Dürrast 2014).

Petrographic and scanning electron microscope analysis were made to analyze the microfibrils and microcracks before and after the salt crystallization test. X-ray diffraction of whole rock samples was used to determine the mineralogical and geochemical composition.

Results

Stone classification and description

The plutonic stones in this study are classified in general as monzogranites and granodiorites, with the exception of two gabbros (TT Black and Black Singoish) and one tonalite (Indian Black) (Table 1). With the exception of the P1, all are phaneritic and equigranular. The sample P1 can be classified as a porphyritic granite due to the bimodality between the matrix formed by quartz and feldspars (grain size of

Table 1 Normalized composition (*based on CIPW norm) and respective Streckeisen's classification

Sample names	Colors	Normalized composition (%)			Streckeisen's classification
		Q	A	P	
Amarelo Real (AR1)	Yellow	38.1	28.8	33.1	Monzogranite
Branco Micaela (BM1)	Gray	30.8	40.7	28.5	Monzogranite
Branco Real (BR1)	Gray	36.4	30.7	32.9	Monzogranite
Mondim de Basto (MB1)	Yellow	37.9	31.5	30.6	Monzogranite
Mondim de Basto (MB2)	Yellow	37.6	32.3	30.1	Monzogranite
P1*	Gray	40.4	39.4	20.2	Syenogranite
P2*	Yellow	41.7	30.4	27.8	Monzogranite
P3*	White	37.8	32.5	29.7	Monzogranite
P4*	Yellow	37.6	33.3	29.2	Monzogranite
Puerto ALP*	Yellow	36.5	31.4	32.1	Monzogranite
Indian Gold*	Yellow	35.2	23.7	41.1	Gneiss
Indian Black*	Black	21.9	0.0	78.1	Tonalite
TT Black*	Black	16.1	0.0	83.9	Gabbro
G603*	Gray/pink	36.1	27.3	36.6	Monzogranite
G654*	Black	25.3	10.3	64.4	Granodiorite
G682*	Reddish	31.0	35.9	33.1	Monzogranite
G603new*	Gray	29.5	23.3	47.2	Granodiorite
G341*	Gray	26.4	23.7	49.9	Granodiorite
Black Singoish*	Black	16.6	0.0	83.4	Gabbro
Paradiso*	Red	28.9	7.6	63.5	Gneiss
Viscount*	Gray	29.4	12.4	58.2	Gneiss
Verde Bahia*	Green	32.1	33.7	34.3	Charnockite
Candeias*	Green	31.4	23.5	45.1	Monzogranite
TQ1*	Yellow				Monzogranite
V2*	Gray	28	22	49	Granodiorite
V1*	Gray	34	34	33	Monzogranite
Flossenburg*	Yellow	37.3	31.8	30.9	Monzogranite
Walenstein*	Yellow	34.1	34.8	31.1	Monzogranite

around 0.25 cm) and the orthoclase phenocrystals with a size around 1 cm. The samples MB1, MB2, AR1, BM1, BR1, Flo, Wal, P1, P2 and P4 are coarse grained. G603, G603new, V1, V2, G682, TT Black, P3, TQ1 and G654 are medium grained. Indian Black and Black Singoish are fine grained.

The main mineralogical constituents of these stones are quartz, plagioclase and alkali feldspar. Biotite and muscovite are also recognizable. Accessories minerals such as titanite and apatite are present. The secondary minerals mostly consist of micas, like sericite, and iron oxides. Transgranular and intergranular cracks are common in the most weathered stones. Quartz is subhedral to anhedral and most of the mica and feldspars are euhedral to subhedral. The high weathering level in some samples is due to the alteration of feldspars by the formation of secondary white micas and also by microcracks filled with iron oxide. Samples P1, P2 and MB1 are

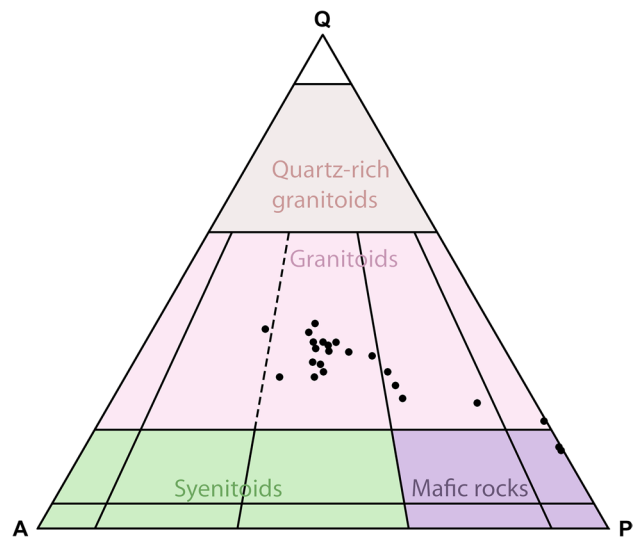


Fig. 5 Petrographic classification according to Streckeisen (1976) of all studied plutonic rocks given in Table 1 (composition from CIPW norm)

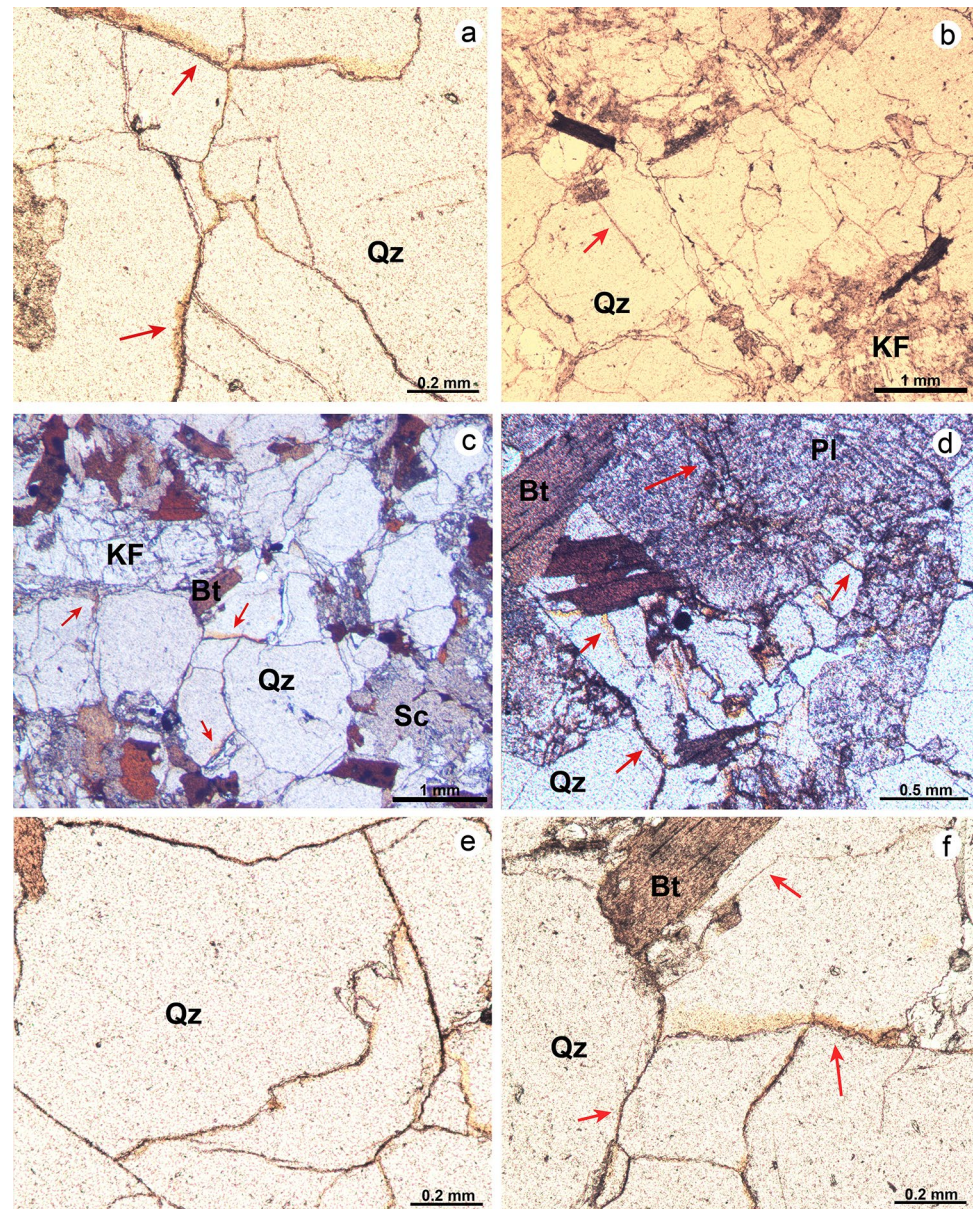
characterized by a large amount of transgranular and intergranular microcracks.

The petrographic analysis of the stone aids in identifying the main factors of importance in regard to the rock behavior with respect to weathering and crack characteristics. The most important mineralogical and microstructural characteristics for some selected rocks are presented below. The mineralogical composition was assessed visually and is only a rough estimation.

MB1 and MB2

Stone with a dominate yellow color, equigranular with a coarse grain size. A porphyritic tendency is found in some samples. The mineral composition is quartz (35%), orthoclase (25%), plagioclase (25%), muscovite (8%), biotite (4%) and microcline (3%). Apatite, zircon, opaques, sericite and iron oxides are present in low quantities. The grain contact with frequent cracks is irregular and lobate. The quartz crystals are anhedral to subhedral in shape, have a grain size between 2 and 4 mm and show an undulose extinction. A large amount of outlined intragranular and transgranular cracks are sometimes filled with iron oxide (Fig. 6a). Alkali feldspars are mainly orthoclase but microcline is also present. They are predominately subhedral in shape with a mean grain size of 6 mm, show inclusions of opaque minerals and a high degree of intergranular sericitized cracks. The plagioclase has a mean grain size of 4 mm and biotite intergrowth and intergranular cracks were observed on the grain boundaries. Biotites are subhedral, and mainly observed in sections perpendicular to the cleavage. The MB1 variety

Fig. 6 The most weathered granites shows a high degree of cracking: MB2 (a), Puerto ALP (b), P1 (c), P2 (d, e) and P4 (f)



have the same characteristics as the MB2 sample, but shows a higher degree of weathering.

Puerto ALP

This stone has a dominate yellow color and is inequigranular with a medium grain size. The mineral composition is quartz (35%), plagioclase (27%), microcline (17%), orthoclase (14%) and biotite (6%). Apatite, zircon, opaques, sericite and iron oxides are present in low amounts. The contact between the grains is interlock, interlobate, with frequent cracks (Fig. 6b). Quartz is anhedral with a mean grain size of 3 mm, shows inclusions of opaques, apatite and sometimes biotite. Plagioclase is subhedral in shape, often with muscovite. Some grains show vermiform quartz intergrowths

(myrmekite) in contact with alkali feldspars. K-feldspars are subhedral in shape and orthoclase exhibits more inclusions of sericite than the microcline. Orthoclase is 3–4 mm in size, show typical Carlsbad twinning and intragranular cracks. Microclines are 2–3 mm in size, exhibit the typical tartan pattern, intragranular cracks and biotite inclusions. Biotites are subhedral to euhedral, have a mean grain size of 2 mm and inclusions like zircon and opaque minerals.

G654

Stone with a dominate black color, is inequigranular and fine- to medium-grained. The mineral composition is plagioclase (57%), biotite (20%), quartz (15%), orthoclase (8%) and hornblende (3%). Low quantities of apatite, zircon,

opaque minerals, sericite and iron oxides are present as secondary and accessory minerals. The contact between the grains is linear and interlobate. Plagioclase is the main component of the matrix, has a euhedral shape and a grain size of 2 mm, showing opaque inclusions, intragranular cracks subparallel to the cleavage and transgranular cracks. Biotite has a grain size of 2 mm, is subhedral in shape and displays inclusions of opaques and zircons. Quartz is anhedral in shape and has a mean grain size of 3 mm, with inclusions of opaque minerals and apatite and displays transgranular and intragranular cracks rarely filled with iron oxide. Orthoclase has a euhedral to subhedral shape with a low level of sericitization. Hornblendes are subhedral to euhedral in shape, contain opaque inclusions and cleavage planes filled with iron oxide.

V1

This stone shows a dominate gray color, is equigranular and medium grained. The mineral composition is quartz (31%), orthoclase (28%), plagioclase (31%) and biotite (8%). Apatite, opaque minerals, sericite and iron oxides are present in low amounts. The contact between the grains is mainly interlobate and sometimes linear. Quartz has an anhedral shape and a mean grain size of 4 mm. It displays intragranular cracks sometimes with recrystallization in the border of other quartz grains. Quartz also has some opaque minerals and fluid inclusions, and shows intragranular and transgranular cracks occasionally filled with iron oxide. Orthoclase ranges in size from 3 to 4 mm and occasionally shows perthitic texture and rarely sericite. The crystals are subhedral in shape and contain intragranular cracks, mostly subparallel to the cleavage. Zoned minerals are also observable. Plagioclase is 2–3 mm in size, is subhedral to euhedral in shape and scarce biotite growth and weathering signals are visible. Biotites are 1–2 mm in size, normally euhedral to subhedral, with inclusions of opaque minerals and apatite.

P1

Gray to yellow colors dominate this stone, is porphyritic with phenocrystals of orthoclase and coarse- to medium-grained. The mineral composition is quartz (38%), orthoclase (30%) plagioclase (10%), biotite (17%) and muscovite (5%). Low amounts of apatite, opaques, sericite and iron oxides are present. Besides the porphyritic texture, the high degree of weathering and cracking are the main features of this stone. The contact between the grains is mainly interlobate and squeezed close to the phenocrystals. Anhedral quartz has a mean grain size of 2.5 mm and displays frequent transgranular, intragranular and intergranular cracks, which are mostly filled with iron oxide (Fig. 6c). Orthoclase is present as phenocrystals with a mean grain size of 12 mm, but

also with smaller grains of 1 mm. The phenocrystals show some perthite and opened cracks sub-perpendicular to the cleavage and medium to low sericitization. Plagioclase is subhedral in shape and is about 2 mm in size. Biotites usually show an anhedral shape, squeezed contacts surrounding the grains of quartz and shows alignment to the phenocryst growth.

P2

The dominant color of the stone is yellow and red, inequigranular, and coarse to medium in grain size. The mineral composition is quartz (40%), alkali feldspar (35%), plagioclase (15%), biotite (5%) and muscovite (3%). Apatite, opaques, sericite and iron oxides are present as secondary and accessory minerals. This stone has a high degree of weathering and many cracks are present (Fig. 6d, e). Quartz has an anhedral shape and is 3–5 mm in size, heavily crossed by transgranular and intergranular cracks frequently filled with iron oxide. Orthoclase is subhedral in shape and displays sericite and intragranular and transgranular cracks. Plagioclase shows some muscovite overgrowth and intragranular cracks. Biotites are euhedral in shape and iron oxide deposition occurs around the grain boundaries.

P3

This stone is white to yellow in color, equigranular, and medium- to fine-grained. The mineral composition is quartz (34%), plagioclase (30%), orthoclase (22%), microcline (8%), biotite (4%) and muscovite (3%). Secondary white micas and iron oxides as well apatite and opaques are present. It shows intermediate degrees of weathering and cracking. The contact between the grains is mainly interlobate and interlock. Quartz has an anhedral shape and a mean grain size of 2.5 mm, displaying transgranular and intragranular cracks filled with iron oxide. Orthoclase shows a subhedral shape and is 2.5 mm in size, showing sericite, opaques and intragranular cracks. In the contact between alkali feldspar and plagioclase myrmekite intergrowth is often visible. Plagioclase is around 2 mm in size and is also weathered, showing many cracks. Biotites with a size of 1.5 mm are euhedral to subhedral in shape and displays inclusions of opaque minerals and apatite.

P4

The dominant color in this stone is yellow, is coarse grained and has a porphyritic tendency. Display intermediate weathering features. The mineral composition is orthoclase (34%), quartz (31%), plagioclase (20%), microcline (5%), biotite (4%) and muscovite (4%). Sericite, iron oxides, chlorite, apatite and opaques are present in low amounts. The contact

between the grains is mainly interlobate and interlock. Quartz has mean grain size average of 4 mm and is anhedral in shape, and displays intragranular cracks sometimes filled with iron oxide (Fig. 6f), which are more frequent than transgranular cracks. Orthoclase is subhedral and shows a grain size of about 8 mm. It exhibits transgranular cracks sub-perpendicular to the cleavage and sericite overgrowths. Plagioclase (3 mm in size) shows weathering features, is subhedral in shape and has biotite overgrowths and intragranular cracks. Biotites are euhedral, with a size of 2–3 mm, and contain inclusions of apatite, zircon, iron oxide and opaques. Chlorite showing a low interference green–blue color is present and indicates biotite weathering.

G603

Stone with a dominate gray and pinkish color, is inequigranular and medium-grained. The mineral composition is orthoclase (35%), plagioclase (33%), quartz (25%), microcline (5%) and biotite (5%). Zircon, opaques, white micas and iron

oxides are also present. The contact between the grains is mainly interlobate. Orthoclase has two main grain sizes, the first one is anhedral with a grain size of ca. 5 mm, sericitized and with intragranular cracks. The second has a grain size of ca. 3 mm with a rounded form and exhibits exsolutions of plagioclase. Plagioclase is subhedral to euhedral and has a grain size of around 3–4 mm, sometimes shows zonations and intragranular cracks. Quartz is anhedral with a size of 4 mm, exhibiting intragranular cracks and few transgranular cracks. Biotite is euhedral in shape, has a grain size of ca. 2 mm, and zircon and opaques as inclusions.

Porosity, density, saturation coefficient, water vapor diffusion resistance and pore radii distribution

The porosity is an important property which gives an indication of the amount of stone volume occupied by pores and cracks. For this reason, this property has a direct effect on the weathering characteristics (Table 2). A first grouping of studied samples can be generated by considering the

Table 2 Obtained values of porosity, bulk density, matrix density, saturation coefficient (S), capillary water uptake (CWU) and water vapor diffusion (WVD) resistance

Stones	Porosity (%)	Bulk density (g/cm ³)	Mtx density (g/cm ³)	S (–)	CWU (kg/m ² /h ^{1/2})	WVD (–)
Black Singoish	0.10	2.95	2.95	0.61	0.39	881.01
Indian Black	0.11	3.05	3.05	0.93	1.60	474.39
Candeias	0.26	2.67	2.68	0.89	0.43	244.99
Viscount	0.27	2.64	2.65	0.88	0.09	162.90
Verde Bahia	0.27	2.66	2.67	0.74	0.34	411.14
G654	0.33	2.77	2.78	0.78	0.45	183.70
TT Black	0.35	2.85	2.86	0.79	0.72	182.53
Paradiso	0.54	2.68	2.70	0.75	0.33	155.85
V2	0.61	2.65	2.66	0.91	0.67	
V1	0.70	2.67	2.69	0.78	0.58	
BR1	0.72	2.62	2.64	0.99	0.79	179.28
Puerto ALP	0.90	2.64	2.67	0.79	1.48	134.90
BM1	0.91	2.60	2.63	0.72	0.35	329.54
Indian Gold	1.02	2.61	2.64	0.81	0.49	83.18
AR1	1.04	2.63	2.66	0.99	1.63	244.59
G603new	1.05	3.04	3.08	0.75	0.27	296.70
G603	1.37	2.59	2.63	0.62	1.11	273.23
P4	1.39	2.62	2.65	0.79	0.98	177.29
G341	1.41	2.65	2.69	0.52	0.31	149.33
P3	1.50	2.60	2.64	0.89	1.15	140.16
Flo	1.59	2.62	2.66	0.74	1.07	127.53
Wal	1.73	2.62	2.66	0.71	0.74	150.94
TQ1	1.86	2.61	2.66	0.94	1.70	284.01
G682	1.91	2.57	2.62	0.56	1.60	176.92
MB2	2.70	2.88	2.96	0.73	1.73	119.09
MB1	2.81	2.35	2.41	0.69	1.58	87.56
P1	4.30	2.56	2.67	0.67	1.83	79.58
P2	4.75	2.53	2.65	0.74	1.74	83.42

total variation between a minimum value of 0.10% for Black Singoish and a maximum value of 4.75% for P2. The mean value obtained for all the stones is 1.3%. The bulk density is related to the mineral composition. In this collection, the bulk density ranges between a minimum of 2.35 g/cm³ for the stone MB1, and a maximum of 3.05 g/cm³ for the stone Indian Black, with an overall mean value of 2.68 g/cm³.

Although the porosity and density define the basic parameters of the stone physical properties, the saturation coefficient allows the frost resistance to be evaluated. It is directly related to the porosity, because it gives the relation between the water absorption under atmospheric conditions and the absorption under vacuum conditions. The samples studied have a saturation coefficient of 0.99 (maximum value) for the samples P1 and P2 and a minimum of 0.52 for the Black Singoish sample, with a mean value of 0.78.

The WVD provides a numerical value of the diffusion resistance of a building material when compared to a static air layer of the same thickness (Siegesmund and Dürrast 2014). This figure is usually related to porosity and pore radii distributions, and therefore, is of great importance for the durability of the stones. The values of the WVD resistance ranges from 79.6 (Paradiso) to 881.0 (Black Singoish), with a mean value of 223.6.

The pore radii distribution is one of the most important parameters considered for stone conservation studies because of the association with porosity and water absorption (Siegesmund and Dürrast 2014). This property is valuable for rock characterization despite some disturbance occurring during the injection of the mercury (Anovitz and Cole 2015), with a slight increase in porosity values (Sousa et al. 2017). The distribution of pore sizes can be divided into three types: unimodal, unequal unimodal, and unequal bimodal (Ruedrich and Siegesmund 2006). The first one shows a distribution in a narrow pore size. In the second type, one unequal maximum is visible. The third one shows one sub-maximum (see Siegesmund and Dürrast 2014). The pore radii distribution also allows the identification of the relative importance of the micropores and capillary pores (macropores). The first one varies between 0.001 and 0.1 µm and the second one ranges from 0.1 µm and 1 mm (Klopper 1985). In this study two groups are defined: micropores (less than 0.1 µm) and macropores (more than 0.1 µm).

The mean value of pore size varies between a minimum of 0.04 µm for the stone G603new and a maximum of 11.72 µm for the sample G682, with an overall mean of 1.54 µm (Table 3). The more abundant size class for almost all the stones is located between 0.1 and 1 µm. As a common situation the percentage of macropores is higher than micropores. Only the samples MB1 and G645 have 100% of the volume of pores in the macropores field. Indian Gold, Viscount and Paradiso samples have a similar distribution of macropores and micropores. The only sample with

percentage of micropores clearly higher than macropores is G603new, with 65.1 and 34.9%, respectively (Table 3).

The unequal bimodal distribution is the more common in the investigated stones, with the maximum located in the macropores field and the sub-maximum usually in the same field. The unimodal distributions are rare and they have low frequency. From our collection, 20 distributions were classified as unequal bimodal, three samples can be classified as unequal unimodal (G654, TQ1 and V1). Five samples do not have a distinguishable distribution due to the low porosity (Black Singoish, Candeias, Indian Black, Verde Bahia and Viscount), but are between the unequal unimodal and the unequal bimodal. In Fig. 7 some examples of pore radii distributions are presented.

Capillary water absorption

The water absorption is related to the porosity, while the size and connectivity of the pores also controls the rate of absorption (Siegesmund and Dürrast 2014; Karagiannis et al. 2016). Usually the absorption curves have an initial portion where the absorption is fast, followed by the stabilization on the curve on the graph water absorption-time (Siegesmund and Dürrast 2014; Çelik and Kaçmaz 2016; Karagiannis et al. 2016; Feijoo et al. 2017; Barroso et al. in press).

Generally, the more porous stones rich in micropores are, the more water they absorb and quickly. The dynamic of the absorption is similar for the stones presented in Fig. 8, but the most porous (e.g., P1, P2, MB1 and Flo) reach more than 90% of the weight absorption in 2 h. The sound granites with a crack pattern, less dense and interconnected, needs much more time to reach the same weight proportion. The stones with porosity values between those two groups also present an intermediate behavior.

This dissimilar behavior can be easily seen in monuments or buildings where stones with high porosity show a wet front located several meters above the floor. This is where the water source is located, stimulated by the cycles of capillary-rising moisture (Moreno et al. 2006; López-Arce et al. 2011). In Fig. 9 is notorious the evolution of the capillary fringe when the stones are placed in a water table, with a more rapid evolution in porous ones. The stones MB2 (2.37%) and MB1 (2.57%) show the highest water suction, which took about 4 h to reach the top of the cubes. The less porous stones, G603 (0.53%) and G654 (0.15%) show a small capillary fringe as expected.

In the studied stones, the coefficient of capillary water uptake (CWU) ranges from 0.02 kg/m² h^{-1/2} in Indian Black to 1.83 kg/m² h^{-1/2} in P1, with an overall mean of 0.87 kg/m² h^{-1/2}. Are not identified differences in CWU among the three directions. Freire-Lista and Fort (2017) only mention significant differences in CWU values after a capillary test

Table 3 Pore radii distribution, mean pore radii and percentage of micropores (0.001–0.1 μm ; % Micr) and macropores (0.1 μm –1 mm; % Macr)

Stones	0.001– 0.01 μm (%)	0.01–0.1 μm (%)	0.1–1 μm (%)	1–10 μm (%)	10–100 μm (%)	Mean (μm)	% Micr	% Macr
Black Singoish	0.0	17.7	23.6	8.4	50.3	2.6	17.7	82.3
Indian Black	0.4	13.0	39.5	8.4	38.8	1.6	13.4	86.6
Candeias	0.0	6.6	38.1	8.9	46.4	2.5	6.6	93.4
Viscount	35.0	20.3	18.2	5.5	21.1	0.1	55.3	44.7
Verde Bahia	16.1	19.2	26.7	9.8	28.3	0.4	35.3	64.7
G654	0.0	0.0	25.0	59.6	15.4	2.1	0.0	100.0
TT Black	0.0	23.9	40.9	14.3	20.9	0.5	23.9	76.1
Paradiso	33.7	14.4	31.2	2.9	17.8	0.1	48.1	51.9
V2	0.0	1.5	20.8	36.4	41.3	5.0	1.5	98.5
V1	0.0	6.5	24.8	52.9	15.8	1.0	6.5	93.5
BR1	0.0	3.4	33.7	24.3	38.6	3.1	3.4	96.6
Puerto ALP	0.0	0.0	39.9	43.4	16.7	1.8	0.0	100.0
BM1	0.0	5.2	24.5	37.8	32.5	2.8	5.2	94.8
Indian Gold	35.9	19.1	30.7	5.2	9.1	0.1	55.0	45.0
AR1	19.0	16.8	22.9	15.7	25.6	0.4	35.8	64.2
G603new	49.5	15.6	20.6	5.3	9.1	0.04	65.1	34.9
G603	0.0	5.2	58.1	29.4	7.3	0.7	5.2	94.8
P4	0.0	12.5	72.3	15.2	0.0	0.3	12.5	87.6
G341	10.8	26.3	47.5	4.2	11.2	0.2	37.1	62.9
P3	5.8	8.9	53.7	22.2	9.3	0.5	14.7	85.3
Flossenburg	1.0	31.6	22.4	37.0	7.9	0.5	32.6	67.4
Waldstein	0.0	11.1	53.3	35.7	0.0	0.6	11.1	88.9
TQ1	0.0	10.9	72.5	7.9	8.7	0.4	10.9	89.1
G682	0.0	2.8	19.4	5.0	72.9	11.7	2.8	97.2
MB2	0.0	5.7	54.8	19.7	19.9	1.2	5.7	94.3
MB1	0.0	0.0	39.9	43.4	16.7	1.9	0.0	100.0
P1	0.0	21.3	48.4	25.8	4.4	0.4	21.3	78.7
P2	3.5	11.6	49.7	21.0	14.3	0.6	15.1	84.9

during a period of 38 days. Vázquez et al. (2010) found significant differences in granites with preferable and visible crack orientation.

Salt crystallization test

The dynamic between crystallization and dissolution cycles produce weight loss, especially detaching of the mica and quartz, a change in the size of the grains, change in the size of the pores and visible surface deterioration. For the most weathered stones, the evolution can be observed with the naked eye, by the increased roughness because of the loss of material, especially in the sample corners (Fig. 10). In sound granites, the salt action is more difficult to distinguish and the increase of the roughness is more evident than weight loss (Alonso et al. 2008). The most common way to visualize and access of these complex effects is by measuring the weight loss of the samples.

The number of salt tests carried out was at least 59, but for some samples 127 cycles were performed (Table 4).

Once the samples were submitted to different number of cycles the comparison can only be done for 59 cycles. The samples MB2, MB1, Puerto ALP, Flo, Wal, P1, P2, P3 and P4 have at least a diminution of 1% in their weight. The samples AR1, G654, G341, Indian Gold and TQ1 have measurable weight changes. All the rest of the samples do not show weight diminution at the 59th cycle. However, when we look for the evolution of the samples subjected to a high number of cycles a more evident weight change occurs after the 80th cycle (Fig. 11). A close view (Fig. 12) of the samples with more weight loss in the first 59 cycles show a similar evolution with the MB2 sample, one with the worst behavior after 127 cycles. Considering the evolution of the sample MB2 (see Fig. 11), the other weathered samples will have a worse evolution, i.e., with

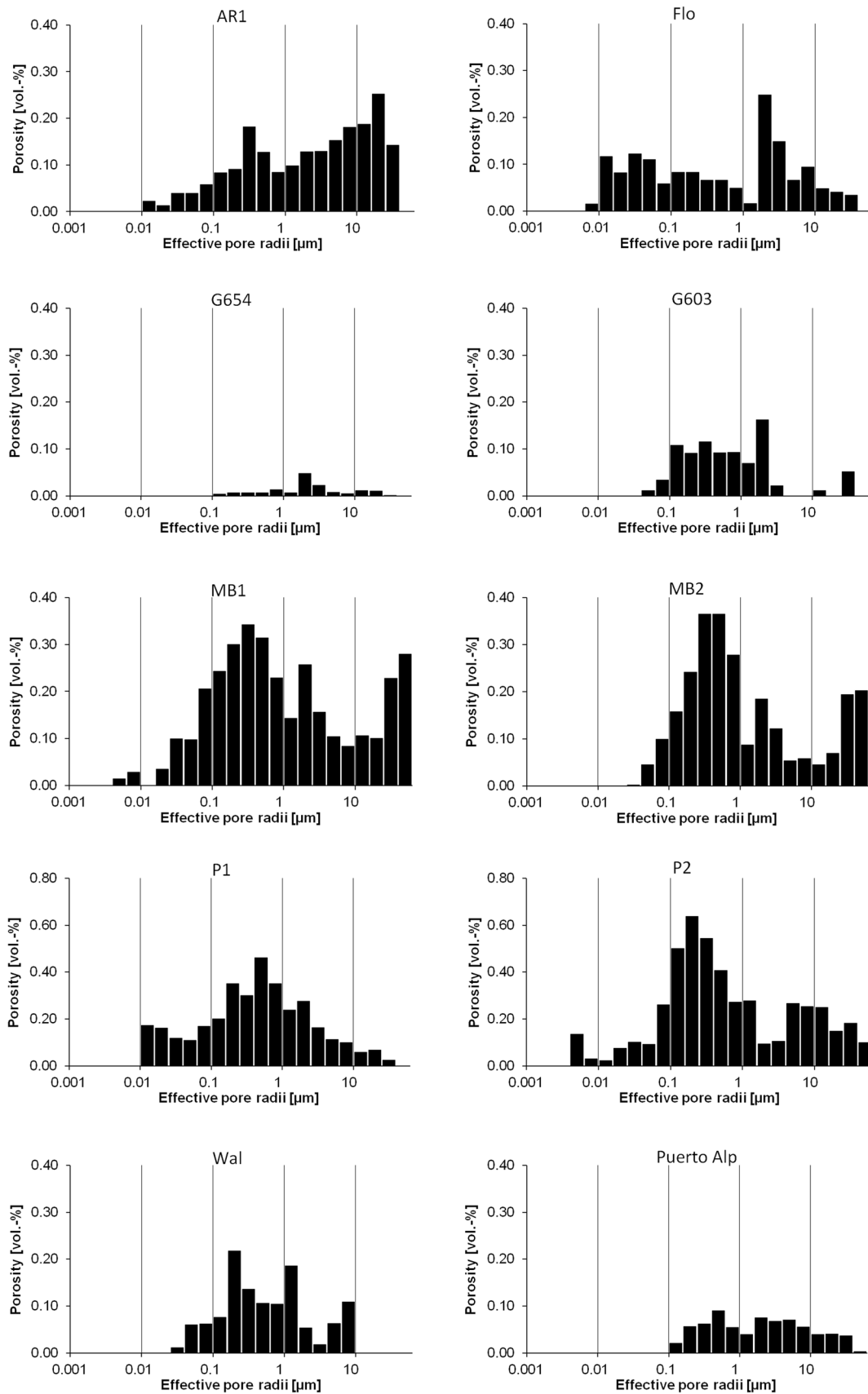


Fig. 7 Pore radii distribution of selected stones. The unequal bimodal is the most frequent pore radii distribution

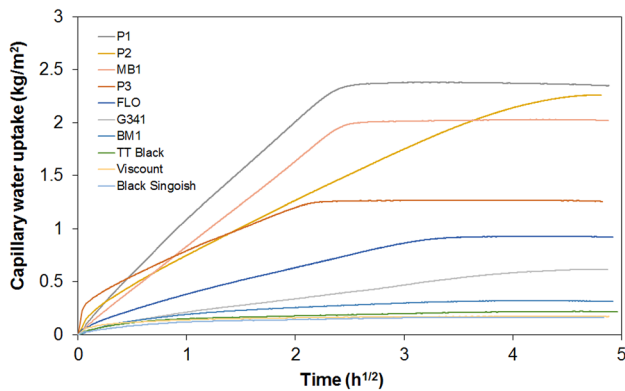


Fig. 8 Different pattern curves of water absorption during the capillary water uptake test

more weight loss. It means that after 130 cycles all these samples will have a weight loss higher than 15%.

Also evident is the increasing weight during the first 10th–15th cycles resulting from the salt accumulation inside the pore network (Angeli et al. 2007; Thomachot-Schneider et al. 2016; La Russa et al. 2017). The less porous samples do not show this initial weight increase so clearly.

Discussion

Density, porosity, pore radii

The value of bulk density and the matrix density of plutonic stones are normally similar, about 2.65 g/cm^3 (Mosch 2009) due to their expected natural low porosity (Siegesmund and Dürrast 2014). The density mainly depends on the mineralogical assembly as consequence of the atomic weight of each mineral. Therefore, acid rocks have lower density than intermediate and intermediate lower than mafic (Morales Demarco et al. 2011, 2013). In this sense, the values here obtained show a wide range, first, because some of the granites already show some weathering degree, second, because of the different mineralogical assembly. The results obtained in this study are a little higher than the expected for granites, but similar to the values obtained by Mosch (2008) in a study of several different stones types, including plutonic rocks samples (Fig. 13). Stones with mafic minerals obviously have highest values of bulk density (Mosch and Siegesmund 2007).

Samples with the same mineralogical composition have different bulk density values and the porosity plays an important role in these differences as referred in several research studies (Mielke et al. 2016; Khanlar and Naseri 2016; Sousa et al. 2017). Sound granites usually have low porosity (0.5–1%) as observed by several authors (Strohmeier 2003; Hoffmann 2007; Mosch 2009; Morales Demarco

et al. 2013). It is well known that the porosity increases with the weathering degree (Tuğrul 2004). Dultz et al. (2013, b) found fragments of granite in soil with porosities ranging from 7.8 to 22.3%. In this study, the range is higher than the usual found in granitic building stones, since building stones with a high weathering degree were selected. For instance, the samples BR1 and AR1 are from the same quarry but were collected at different depth.

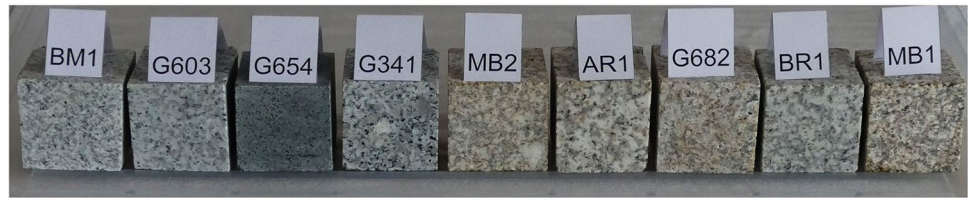
These weathered stones were used more frequently in the urban architecture, not only for the building rehabilitation works but also in new buildings (Sousa et al. 2017). Porosity plays a significant role when it comes to stone weathering and controls the mechanical properties (Siegesmund and Dürrast 2014; Vázquez-Nion et al. 2018; Jamshidi et al. in press). Moisture and fluids can accumulate and flow inside the pores and cause several types of damage (Berrezueta et al. 2017), especially salt decay (Steiger et al. 2014). When the relative humidity decreases, the capillary attraction forces increase and may harden porous rocks (Eslami et al. 2010), but these phenomena do not occur in granitoids and only the negative ones are evident. Therefore, porosity is one of the most important petrophysical parameters and a special attention should be given.

In magmatic rocks, the porosity is related to cracks while the pores in feldspars have a lower contribution, with some exceptional decay weathering forms in basic rocks (Tuğrul 2004; Ceryan 2005). Most available studies of interconnected matrix porosity of magmatic rocks are based on laboratory investigations, i.e., work on samples that have undergone stress relaxation and were affected by drilling and sample preparation (see discussion in Schild et al. 2001 or; Tullborg and Larson 2006). It was found that the unconnected porosity increases in the thicker samples once the contribution of microfractures at the cutting ends is smaller (Tullborg and Larson 2006). Therefore, a special attention during the thin section evaluation is necessary to avoid misleading interpretations. The microscope observations highlight the crack-related porosity as the main impact for the overall porosity. In fact, the cracks containing iron oxides are the most common pore features that contributes to the porosity. This observation is more evident in the most porous and weathered stones such as P2, P1, MB2 and MB1 (see Fig. 6). The texture of the stone, namely the grain size and the foliation influences the intragranular porosity. Sammaljärvi et al. (2017) observed more tortuous and narrow intragranular porosity in a gneiss than in a pegmatite and Pazeto et al. (2017) mention larger cracks around mineral contacts. Some degree of connection between the cracks is a major condition for a water interaction in all the volume of the stone. When the pores are deficiently interconnected the stone absorption and desorption is slower (Feijoo et al. 2017).

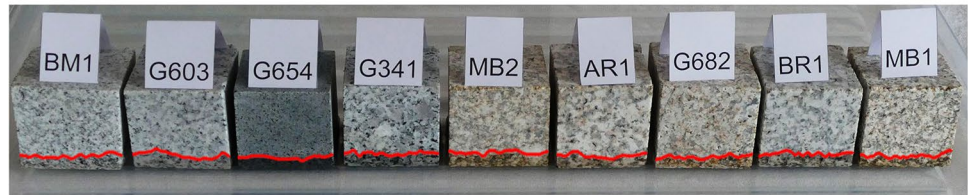
Several classifications have been proposed to classify the stones according to their porosity.

Fig. 9 Evolution of the capillary in some of the studied stones (5 cm cubes; wet limit marked by a red line)

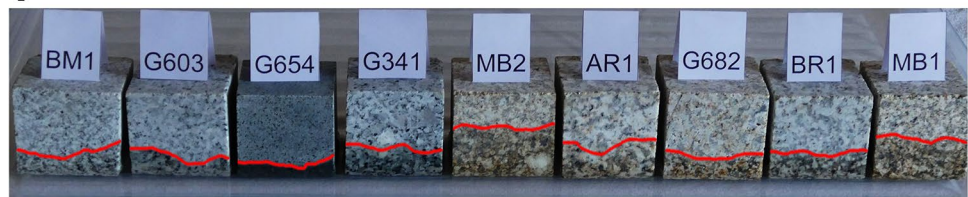
t₀: 0 minutes



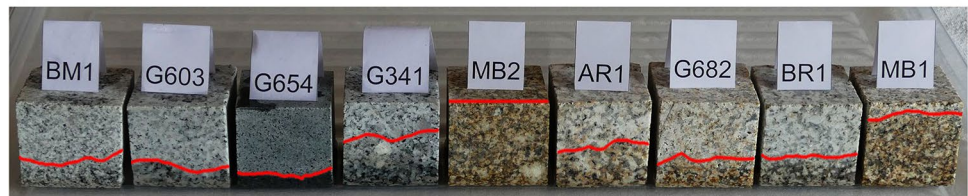
t₁: 1 minute



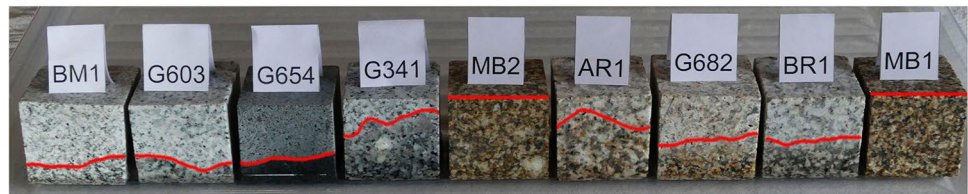
t₂: 60 minutes



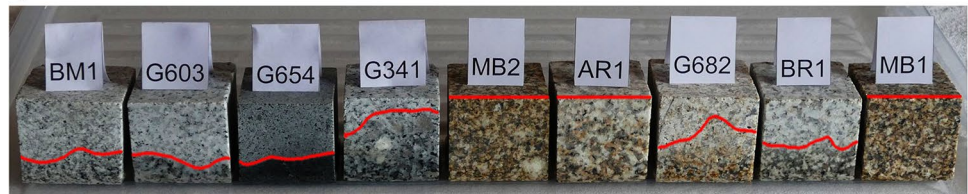
t₃: 4 hours



t₄: 12 hours



t₅: 24 hours



Moos and De Quervain 1948 (in Siegesmund and Snelthage 2014) used the effective porosity to classify the rocks as compact (<1%), with few pores (1–2.5%), as slightly porous (2.5–5%), as significantly porous (5–10%), with many pores (10–20%) and with high amount of porous space (>20%). According to this classification, the stones

in this study are classified as compact (14 stones), with few pores (10 stones) and slightly porous (4 stones). Henriques and Tello (2006) mentioned the following classification for the natural stone used in façades: very low (<0.5%), low (0.5–1.0%), medium-to-low (1.0–3.0%), medium (3.0–6.0%), high (6–10%) and very high (>10%).

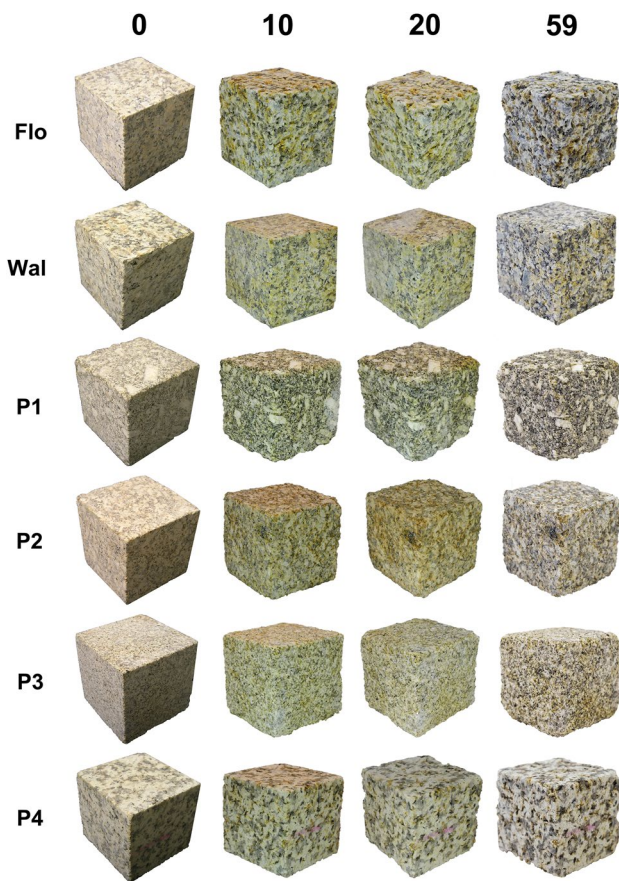


Fig. 10 Evolution of the stones during the salt crystallization test

According to this classification, our set has stones with very low porosity (7), low porosity (6), medium-to-low porosity (13) and medium porosity (2). Also, in the industry of dimension stones some authors mention the 1% of porosity as the suitable limit for the granite (Henriques and Tello 2006; Alencar 2013). Using the 1% of porosity as a limit, only about half of the studied stones (13) have characteristics to be used as building material.

Such classifications and limits should be used with caution because they were defined for different rock types and purposes. Stones carry the decay from the quarry and could be problematic to classify a granite of 2% of porosity as a ‘few pores’ stone. In fact, in the last several decades weathered granites are widely used as building material, however, severe damages were observed on granitoids with porosities higher than 2.0% (Sousa et al. 2017). As a rule, the stones can be used as long they keep the desired quality and durability under the environmental conditions and usage. Establishing a limit, i.e., 1% of porosity, can be misleading for the users given the idea of an unchangeable material. Under special conditions and depending on the agent of decay, even the low porous stones can suffer weathering enough to change the mechanical properties

Table 4 Evaluation of the samples after the salt crystallization test

Stones	Number of cycles	Loss (%)	Loss at 59th cycle (%)
BM1	127	0.0	0.0
AR1		1.9	0.2
BR1		0.0	0.0
MB1		52.0	4.7
MB2		15.0	1.0
V1		0.3	0.0
V2		0.0	0.0
G682		0.2	0.0
G654		0.3	0.3
G603		1.6	0.0
Puerto ALP	70	3.1	3.1
G341		0.5	0.5
TT Black		0.0	0.0
G603new		0.0	0.0
Indian Gold		0.5	0.5
Paradiso	66	0.0	0.0
Verde Bahia		0.0	0.0
Candeias		0.0	0.0
Viscount		0.0	0.0
Black Singoish		0.0	0.0
Indian Black		0.0	0.0
Flossenburg	59	3.6	3.6
Waldstein		1.4	1.4
P1		7.3	7.3
P2		2.4	2.4
P3		3.0	3.0
P4		2.1	2.1
TQ1		0.1	0.1

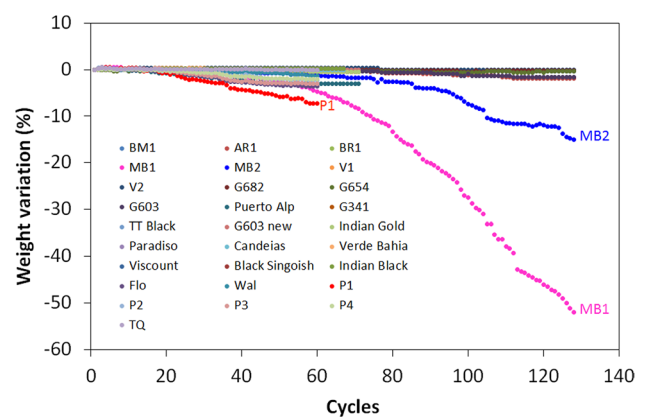


Fig. 11 Behavior of stones during the salt crystallization test. The stones with high loss are marked (P1, MB2 and MB1)

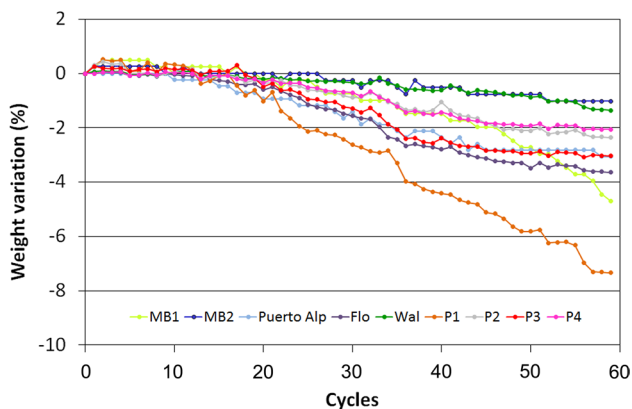


Fig. 12 Weight variation of selected stones during the first 59 cycles of the salt crystallization test

and cause irreversible deterioration, therefore, case by case analyses are necessary.

Pore radii

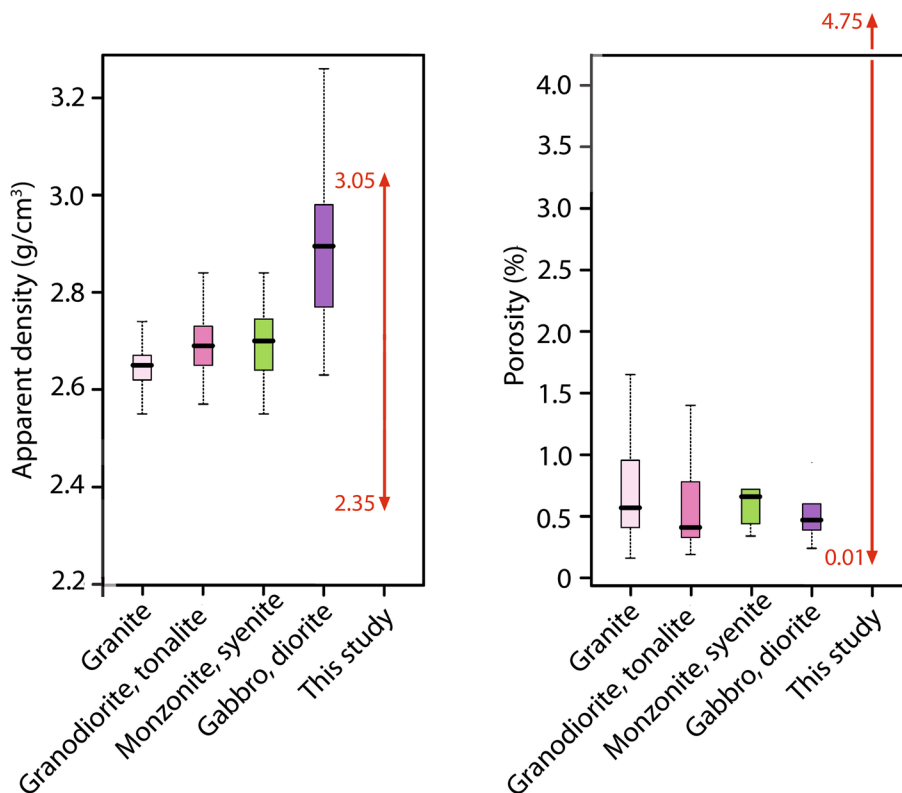
The pore radii distribution is also an important parameter when it comes to stone conservation studies, since it is related to porosity and water absorption and has an essential role in the stone decay (Siegesmund and Dürrast 2014). In this assessment, the detection limit of the MIP technique

(about 0.002 μm) must be taken into consideration (Barbera et al. 2014; Anovitz and Cole 2015; Coletti et al. 2016), however, in granitoids such pore radii size is not frequent. In this study, two main pore radii groups were considered: pores lower than 0.1 μm (micropores); pores higher than 0.1 μm (capillary pores and macropores). The porosity associated to this groups is named microporosity and macroporosity, respectively. For others pore size classifications schemes see Siegesmund and Dürrast (2014).

Several research studies confirm the importance of pore radii distribution in the stones behavior, especially the macropores. In fact, pores with more than 0.1 μm can transport water easily in different phases with consequences on the weathering processes, namely freeze–thaw and salt crystallization (Siegesmund and Dürrast 2014; Çelik and Kaçmaz 2016). In contrast, high microporosity can increase the water retention and lead to dissolution of salt in pores (Wilhelm et al. 2016). The stones with the highest amount of macropores such as MB1, Puerto ALP, G654 and V2 will present a higher capacity to transport water and, therefore, a higher decay capacity. On the other hand, stones with less macropores, like G603new, Indian Gold, G341, Viscount and Paradiso, will have lower susceptibility for weathering.

The pore radii distribution is an important parameter but only when the amount of pores is enough to allow the water action (salt and ice). Considering the percentage of micropores (<0.1 μm) and macropores (>0.1 μm), the microporosity

Fig. 13 Values for density and porosity for plutonic stones and the ones in this study Modified from Mosch (2008)



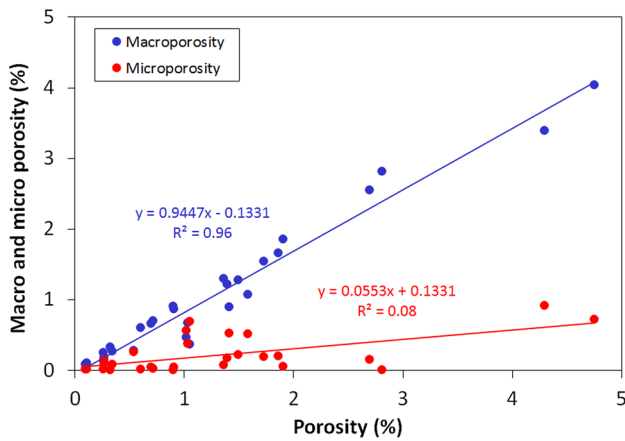


Fig. 14 Contribution of the macroporosity and microporosity for the total porosity

and macroporosity were computed as the respective percentage of the open porosity. As can be seen in Fig. 14, the variation of the porosity is mostly correlated to the macroporosity, which have a mean value of 1.09%, while the mean of the microporosity is 0.22%. The maximum contribution of the microporosity is 0.92% in stone P1 (total porosity – 4.3%). Therefore, stones with higher porosity will also have high macroporosity and consequently more vulnerability to the water action.

The dimension of the pores has a wide range as a consequence of the pore radii distribution and the samples with more macropores obviously will show a higher value of mean pore radii (Fig. 15). As mentioned above, the porosity in these type of stones is crack related (see Fig. 6), which means that the size and the interconnection of the crack network will increase with porosity.

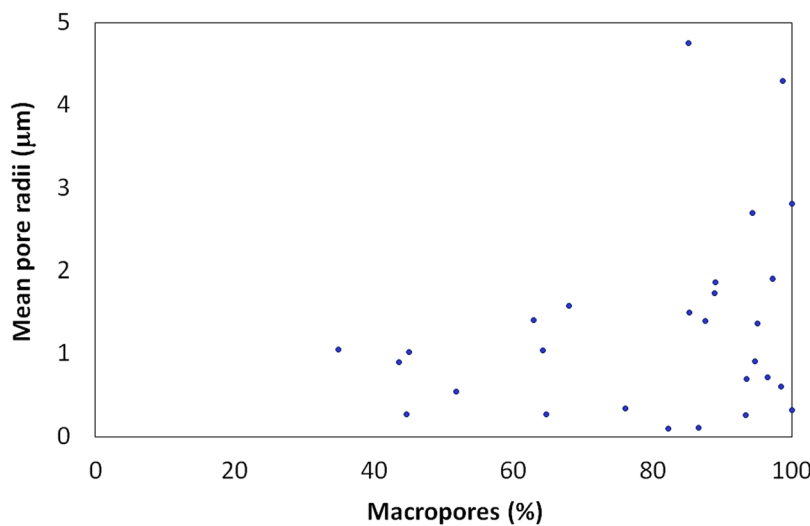
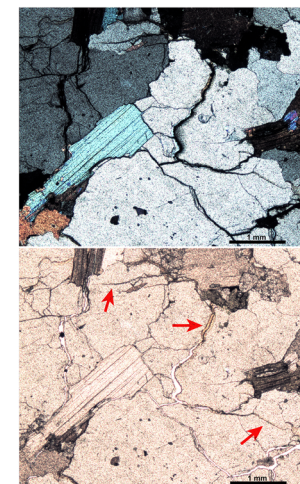


Fig. 15 Relationship between mean pore radii and the percentage of macropores. The photos shows cracks in MB2 granite with oxides



Saturation coefficient

The saturation coefficient defines the percentage of the total pore space accessible to water and is used to evaluate the frost resistance (Siegesmund and Dürrast 2014). As defined by Hirschwald (1912), values under 0.75 indicates a weathering resistant stone, values between 0.75 and 0.9 are not conclusive and further evaluation is necessary, and for values over 0.9 the stone is not weathering resistant. According to this classification, it is possible to classify the samples from this study as is shown in Fig. 16. Thirteen stones are located in the weather-resistant field.

The mean value of the saturation coefficient (0.78) is similar to the mean values obtained by Poschlod (1990), Morales Demarco (2012), Hoffmann (2007) and Mosch (2009), respectively 0.81, 0.85, 0.8 and 0.70. The studied stones have a large range of S values; therefore, the mean

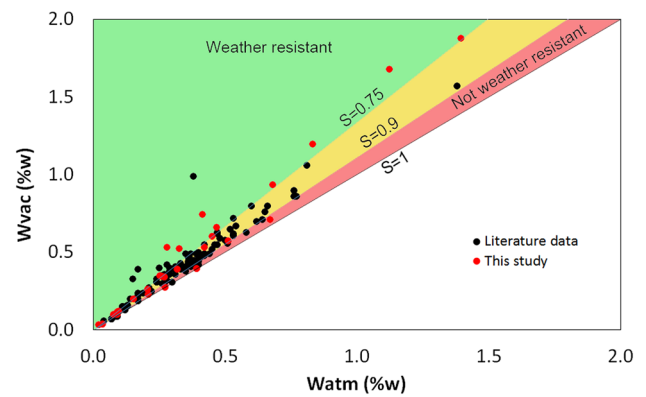


Fig. 16 Classifications of the studied stones according the saturation coefficient (data from Poschlod 1990; Hoffmann 2007; Mosch 2009; Morales Demarco 2012)

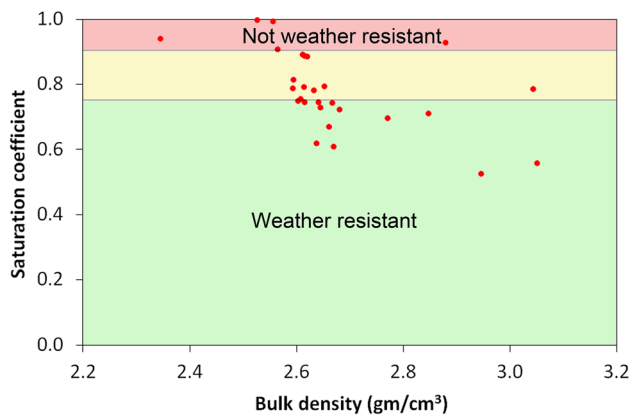


Fig. 17 Relationship between saturation coefficient and bulk density

value could not give a clear image of the frost resistance and the comparisons will be meaningless. Furthermore, in low porous stones the ratio between the water absorption and the forced water absorption (both low values) will provide an inaccurate value. This will be more evident in stones with a bulk density higher than 2.6 g/cm^3 (Siegesmund and Dürst 2014; Morales Demarco 2012). Figure 17 shows there is no relationship between the S value and the bulk density, although the stones classified as weather resistant have a bulk density higher than 2.6 g/cm^3 .

Capillary water uptake

The CWU data of plutonic rocks from the literature (LNEC 1990a, b, c; Pinto et al. 1994; Pérez-Ortiz et al. 1996; Vicente 1996; Begonha 1997; Mosquera et al. 2000; Rivas et al. 2000, 2010; Strohmeyer 2003; Bré 2008; Prieto and Silva 2005; Fojo 2006; Leite 2008; Vázquez et al. 2010; Ferreira 2011; López-Arce et al. 2011; Braga et al. 2012; Silva 2012; Morales Demarco et al. 2013; Feijoo et al. 2013; Mendes 2013; Ribeiro 2013; Antão and Quinta-Ferreira 2015; Sousa et al. 2017) show a range from 0.003 to $11.54 \text{ kg/m}^2 \text{ h}^{-1/2}$, with a mean of $0.83 \text{ kg/m}^2 \text{ h}^{-1/2}$. Despite the differences in the methodological procedures and units used (we have found six different units), the results are similar. The mean value of this study is $0.88 \text{ kg/m}^2 \text{ h}^{-1/2}$. The distribution of the values both in the literature data and new data show a high agglomeration of low CWU values, which is more important in the published data (median values of 0.22 and $0.74 \text{ kg/m}^2 \text{ h}^{-1/2}$, respectively for published and new data) (Fig. 18).

In general, the samples show a higher absorption stage in the first minutes/hours according to the porosity and crack connectivity as observed among all the studies regarding capillary water absorption tests (Mosquera et al. 2000; Karagiannis et al. 2016; Coletti et al. 2016). The stones with higher porosity show higher absorption and reach the

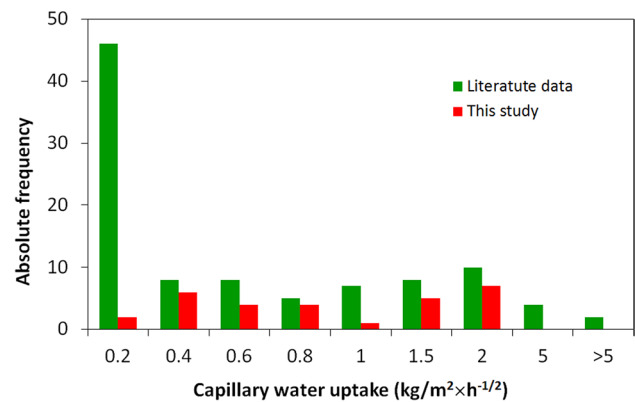


Fig. 18 Histogram of the capillary water uptake of literature data and for this study

maximum of absorption in a short period of time (Siegesmund and Dürst 2014; Çelik and Kaçmaz 2016). The investigated stones are low porous, thereby they should present a general pattern according to their low porosity. However, a closer view shows differences in capillary kinetics.

The capillary absorption curves are a consequence of the pore network and they can be related to the pore radii distribution. For instance, the samples P2 and P3 show two evident sections. The first quasi-vertical stage at the very beginning corresponds to the filling of the interconnected porosity as a consequence of the capillary absorption (Thomachot-Schneider et al. 2008; Karagiannis et al. 2016; Coletti et al. 2016; Feijoo et al. 2017). The next stage is related to the filling of the trapped porosity (Fig. 19). This kind of absorption pattern is related to the bimodal network because the well-connected pores are filled first and the less connected ones are slowly filled (Thomachot-Schneider et al. 2008). The samples MB1 and P1 shows a typical shape for a unimodal porous network, with one uniform stage of weight increase followed by a stable pattern without evident weight variation (Thomachot-Schneider et al. 2008). The arrival of the wet fringe at the top of the sample (see Fig. 9) corresponds to the end of the filling of the free porosity, therefore, the shape of this curve represents a predominate range of well-connected pores. This behavior can also be explained by the amount of microcracks as observed in thin sections (see Fig. 6).

Other samples as Flo and G341 show a continuous increase of water absorption with several slope breaks (Fig. 19). This pattern can be related to the low porosity and the low porous network connection and the fringe does not reach the top of the sample after several hours of testing.

As expected, the CWU values increases with the porosity (Fig. 20) since more space are available to be filled with water. However, the dynamic of absorption can be influenced by the microcrack network and the clay minerals, only to

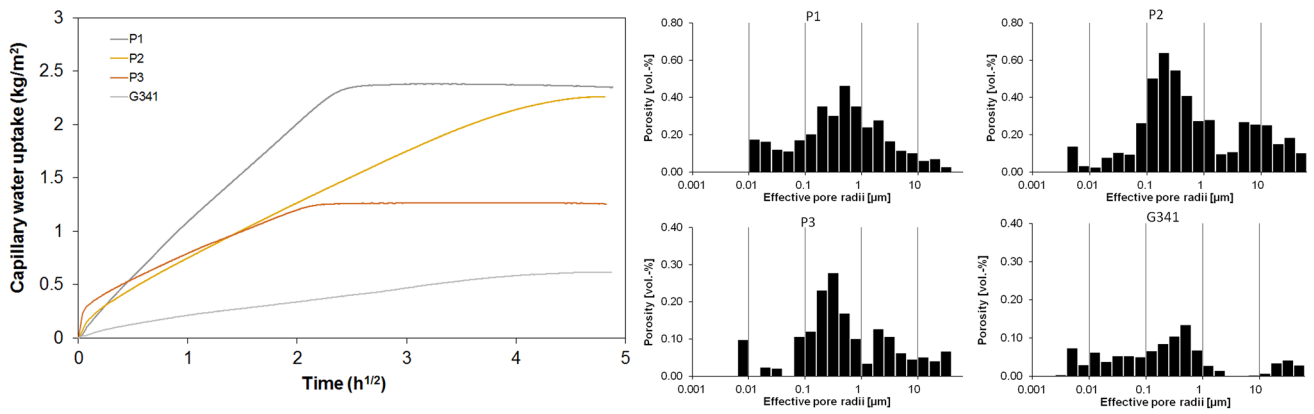


Fig. 19 Relationship between the capillary kinetics and the pore radii distribution

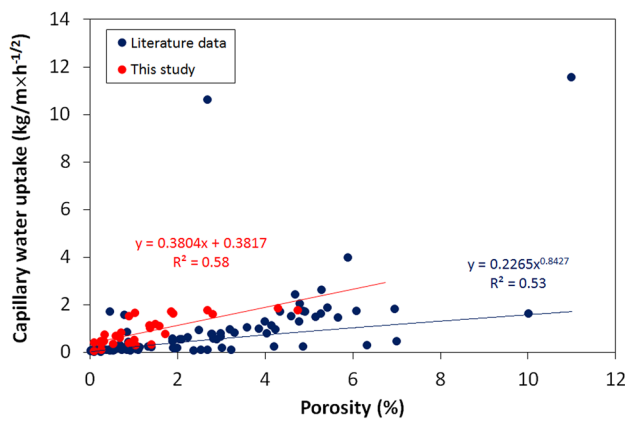


Fig. 20 Relationship between the capillary water uptake and the porosity

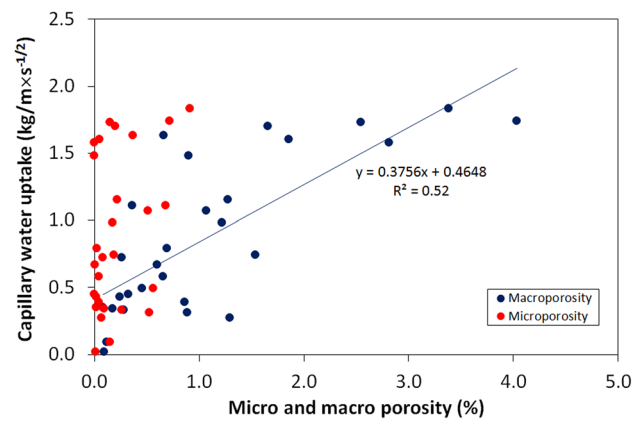


Fig. 21 Relationship between capillary water up take and microporosity/macroporosity

mention some of the possible factors (Sammaljärvi et al. 2017). This relationship is found not only in granitoids but is generally confirmed in all rock types (Graue et al. 2011; Molina et al. 2011; Sengun et al. 2014). Çelik and Kaçmaz (2016) suggest that the combination of a high porosity and a high water uptake has a high damage potential. The macroporosity is the main component of the total porosity, consequently the CWU is also related to pores higher than 0.1 µm (Fig. 21). Once again is emphasized the role of the capillary pores and the macropores on the water absorption and weathering processes.

Apparently, the mean pore radii have no influence on water absorption (Fig. 22). The tortuosity and the connections between the pore network also plays an important role in water absorption and the weathering process (Buj and Gisbert 2010; Yu and Oguchi 2010; Dultz et al. 2013, b; Feijoo et al. 2017). In addition, the pore radii distributions are not equal

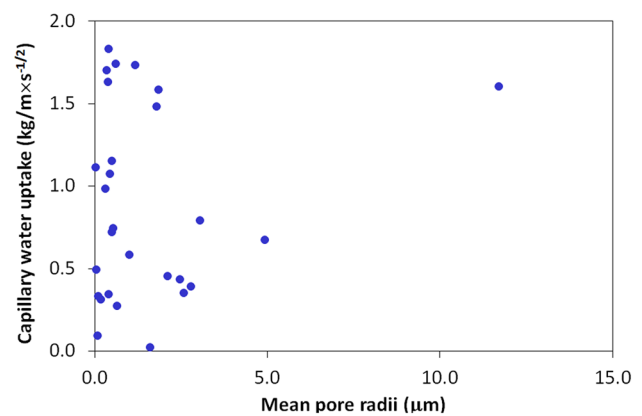


Fig. 22 Relationship between the capillary water uptake and mean pore radii

unimodal as mentioned above, consequently the value of the mean pore radii size is a parameter without a real significance and caution is needed when such values are considered.

Water vapor diffusion

This is an important durability factor and together with capillary absorption represents the two main moisture transport mechanisms. The WVD gives information about the diffusion resistance of a material when in contact with moisture. The highest values of vapor diffusion indicate the higher resistance of the rock to the transport of water in the vapor phase, consequently it also indicates the lowest permeability. In stones with low porosity, the resistance to vapor movement will be high (see Morales Demarco et al. 2011), however, the range of this property on magmatic rocks is highly variable (Strohmeyer 2003; Hoffman 2008; Mosch 2009; Siegesmund and Dürrast 2014). In this research the same occurs, with the high diffusion resistance values in low porous stones (Fig. 23). If the highest (anomalous?) pore radii value is excluded, a tendency for a WVD increase with the pore size can be established. Therefore, the motion of water molecules through the pore space is the preferential diffusion mode (see Siegesmund and Dürrast 2014). Other factors, like the textural and crack anisotropy also plays an important role in the vapor diffusion (Strohmeyer 2003; Hoffman 2008; Mosch 2009), and more detailed studies are necessary for consistent conclusions.

Salt test

Salt weathering as widely known have some typical quantitative and qualitative consequences over the stones surface, namely scaling, flaking, alveolization, back weathering, loss of material (Warke et al. 2011; Vázquez et al. 2013; Siedel and Siegesmund 2014). In the specimens, the loss of material is the most evident consequence of the salt action. The durability of the stones is ruled by important petrophysical

properties, the porous media (porosity and pore size distribution) and the resistance of the rock to pressure crystallization, or simply, the coherence (Benavente et al. 2004, b; La Russa et al. 2017).

The tensile strength and uniaxial compressive strength (UCS) in granitoids are related in a ratio of about 1/10 (Siegesmund and Dürrast 2014; Torkan et al. 2016; Forestieri et al. 2017; Török and Czinder 2017). The published values of UCS for the studied stones have a range between 100 and 200 MPa, therefore, the tensile strength should be between 10 and 20 MPa. The crystallization pressure of the thenardite can reach 13 MPa (Espinosa-Marzal et al. 2011) or even more when a mixture of thenardite and decahydrate occurs in the pores (Saidov et al. 2016). It is difficult to have a measured value of the crystallization pressure; however, the values can be higher than the tensile strength of the stones (Flatt et al. 2017). Consequently, our stones will have a different mechanical strength to salt pressure crystallization. In fact, MB granite with a tensile strength of 12 MPa is more prone to damage than Verde Bahia (19 MPa). After 59 cycles of the salt crystallization test, Verde Bahia have not shown any weight variation, while MB1 has lost 3.7% of material. This last stone loses 29% of material after 100 cycles and 52% after 127 cycles. The more weathered and porous stones also have lower compressive strength, tensile strength and cohesion (Sousa 2004; Ceryan 2005; Momeni et al. 2017), and therefore, will be more affected by salt crystallization (Benavente et al. 2004a, b).

The loss of weight during the salt crystallization test is related to the porosity (Fig. 24). The most porous stone have more cracks for crystal growth and the crystallization pressure is applied commonly with more damage. This relationship is detected in many research studies and is more evident in the high porous stones (Lopez-Doncel et al. 2013; Sousa et al. 2017; Pérez-Fortes et al. 2017). However, in some situations, the voids are larger and they allow crystals to grow without significant pressure on the pore walls (Espinosa-Marzal and Scherer 2008, 2010; Lopez-Doncel et al. 2013;

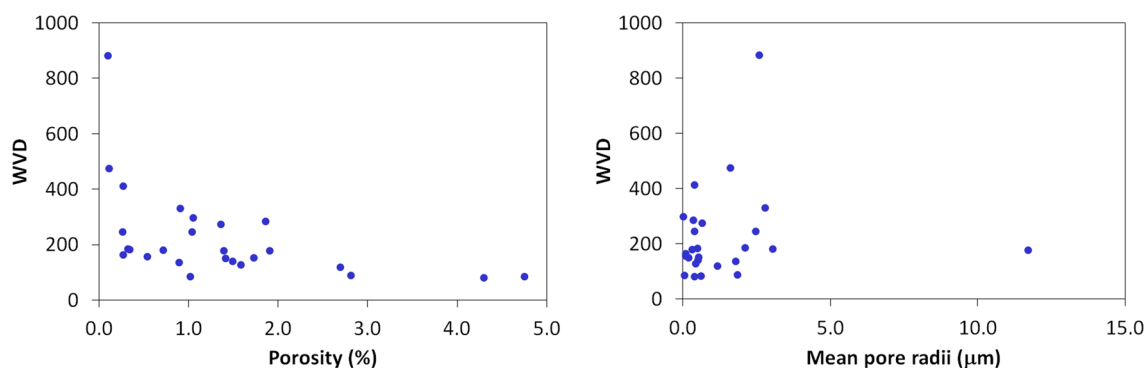


Fig. 23 Relationship between the water vapor diffusion (WVD) resistance and porosity (left) and mean pore radii (right)

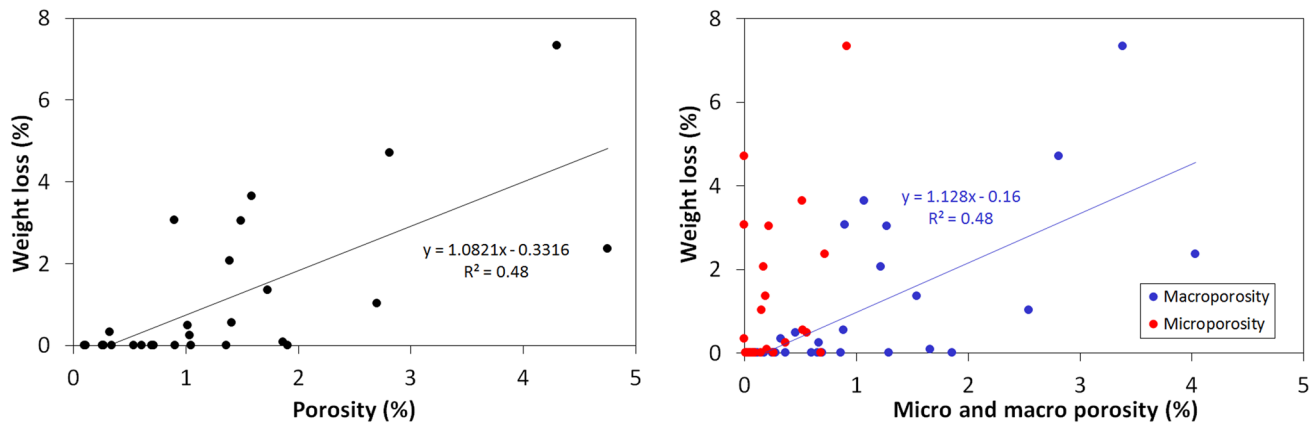


Fig. 24 Relationship between the weight loss at 59th cycle and the porosity (left), microporosity and macroporosity (right)

Steiger et al. 2014; Flatt et al. 2017). It is interesting that the most porous stone (P2) does not show the highest weight loss during the salt test (see Figs. 11, 12) and the low connectivity as discussed above can justify this behavior (see Fig. 19).

Regarding macroporosity, capillary pores and microporosity it was verified that the pore radii distribution plays a considerable role in the most porous stones in this long period salt test (Fig. 24). Stones such as P1, P2, Flo and MB1 have the higher values of capillary pores, macroporosity, and also the highest weight variation. This relationship is expected as a consequence of the relationship between the porosity and these pores (see Fig. 14). The stress is related to the supersaturation and in stones with large pores more salt must precipitate to exert pressure (Espinosa-Marzal and Scherer 2008), therefore, the stones with smaller pores are more susceptible to deterioration (Benavente et al. 2004, b; La Russa et al. 2013, 2017; Steiger et al. 2014; Coletti et al. 2016; Flatt et al. 2017). There are some exceptions when the stones have low pore connectivity and high tortuosity or high porosity (Steiger et al. 2014; MacWilliam 2017). Granitoids have a low pore connectivity and high percentage of capillary pores and macropores, hence the deterioration is mainly controlled by the total porosity, especially in the stones with a high degree of weathering. In our dataset, the porosity is related to the crack network rather than spherical pores as previously stated. The smaller cracks are mainly located inside the crystals (intragranular) and the width is smaller than the intergranular and transgranular ones (see Fig. 6).

Depending on the location in the quarry, weathered granites can have very different porosity values (Sousa et al. 2017) with reflection in salt weathering. For instance, the AR1 granite has a loss of 2.11% after 217 cycles, while a loss of 3.14% after 100 cycles (Sousa 2014) and 4.59% after 70 cycles (Sousa et al. 2017) are mentioned in previous works. In such stones, small variations in the amount

of porosity and in the crack pattern and connectivity will determine high differences in the salt weathering and then a special attention during the assessment of the results is required.

Stones with similar porosity show different susceptibility to the salt test according to the percentage of macropores. For instance, the samples Puerto ALP (porosity 0.9%) and G603new (porosity 1.05%) have different weight variations, 3.6 and 0.0%, respectively. In these stones, the percentage of macropores could be the explanation: 100% in Puerto ALP and 34.9% in G603new. In our dataset, there is no relationship between the mean pore radii and the weight loss.

It is interesting the weight loss pattern of some stones during the salt test. In fact some porous stones do not show evident weight variation after 59 cycles, however, the loosening increases dramatically after 100 cycles probably due to catastrophic crack propagation (see Figs. 11, 12). Obviously, the comparison can only be done for the same number of cycles, but the pattern can be extrapolated for all the stones with similar porosities.

The samples G603 and G603new do not have weight loss after 59 cycles, however, after 127 cycles, G603 have a loss of 1.91%. The size of the pore radii, lower in G603new, the high percentage of capillary pores of G603 (94.8%) and the multimodal pore radii distribution are the reasons for further weight loss in G603. Another unexpected result is the lower weight loss of G682, which with a high porosity (2.7%) only lost 0.2% after 127 cycles. This stone has the higher pore radii size with a non-uniform pore radii distribution besides a high percentage of macropores (97.2%). The stone TQ1, also with high porosity (1.86%), does not lose weight probably because the cracks are sealed with sericite and argillaceous minerals, which makes the movement of free water difficult.

For these low porosity stones, a few number of cycles are not enough to perceive the changes (Alonso et al. 2008;

Vasquez and Alonso 2010; Zedef and Unal 2010), and only after a high number of cycles is the weight decrease notorious. These cycles modify the porous media of the stone and, consequently their petrophysical properties (Benavente et al. 2001; Ludovico-Marques and Chastre 2012; Steiger et al. 2014; Martins et al. 2016; Sousa et al. 2017). Stones with small pores are more prone to clogging (Espinosa-Marzal and Scherer 2013) and this delays the deterioration. The cracks will enlarge due to the crystallization pressure and after a critical number of cycles the internal cohesion decreases and the stones lose material quickly.

For granitoids, the number of cycles to assess the weathering resistance should be at least 100. Lubelli et al. (2014) already suggested the classification of materials according to their durability to salt crystallization, but for low porous stones this cannot be achieved within a short time (see López-Arce et al. 2010). According to Angeli et al. (2007), the most resistant stones during the first cycles are not necessarily the most resistant at the end (see Figs. 11, 12), requiring long-term tests to have a clear illustration of the stone behavior.

Besides the weight loss and roughness increasing, salt action could be also identified by the increasing of porosity. The porosity values of the samples AR1, MB1, MB2, G603, obtained by mercury intrusion, have increased from 1.04, 1.37, 2.81 and 2.70 to 2.01, 2.13, 9.26 and 3.94%, respectively. It is evident that the shift of the pore radii distribution with the increasing percentage of macropores (Fig. 25). López-Arce et al. (2010) mention the increase of the porosity and pore radii size in granites subjected to artificial salt crystallization tests. The increase of macropores is a consequence of the propagation and widening of all the crack types, but especially the transgranular ones as well the development of new cracks (Fig. 25). The stones manifest the salt decay by the open cleavages in micas, pitting on the plagioclase surface, cracks, open grain boundaries, and open coated cracks with iron oxides. Martins et al. (2016) mention that coarse granites are more affected by the salt action, and the larger intergranular cracks in these stones can explain this increase. For the samples with higher porosity such as MB1, MB2, AR1, these features are more evident.

Salt weathering is stimulated by the crystallization of a saline solution absorbed from the outside to the inside of the stone, and what is required is a transport through the pore network by capillarity and diffusion (Sawdy-Heritage et al. 2008; Steiger et al. 2014). If the brine does not fill the porous media completely, the efficiency of pressure crystallization decreases strongly, and therefore, the level of damage will be different and focused on the first millimeters of the surface (Benavente et al. 2004, b; Vázquez et al. 2013). The transport capillary phenomena are more obvious in very porous stones because with large pores the air bubbles can be driven out easily, permitting the solution to completely

fill the pores of the stone (Benavente et al. 2004, b). Thus, once studied stones have different water absorption, differences will occur in the absorption of the saline solution and, consequently, in the damage. For this reason, stones with higher capillary water absorption show a tendency for higher weight loss during the salt crystallization test, however, with a low coefficient of determination (Fig. 26). The connectivity plays an important role in the water absorption and the salt action in low porous stones only can be perceived after a high number of cycles.

Conclusions

To characterize the effect of salt on granite decay, a larger number of granitoid samples were collected and investigated. The collected stones are different in mineralogical composition, microstructure and weathering degree, therefore, the influence of these factors on salt weathering can be assessed. In the recent European standards, the durability of the rocks subjected to salt action is now considered. Salt action is very important in monuments and buildings for heritage maintenance and restoration and wherever porous stones are used as building materials. The growing utilization of porous granites demands a thorough knowledge of their behavior when they are used in wet and cold environments, especially where sodium chloride is used to minimize the ice formation. Sodium chloride is more soluble than sodium sulfate and tends to migrate to the stone surface, causing mainly surface damage. The characterization of the porosity and the behavior of the stones when they interact with water improves the state of knowledge concerning the main factors governing salt action.

As a consequence of the weathering degree, the selected stones have a wide range of porosity, from 0.1 to 4.75%, which corresponds to the cracks. In fact, cracks stained with iron oxides are the most important characteristic of the porosity as observed in the porous and weathered stones (MB1, MB2, P1 and P2). The pore radii distributions are normally unequal bimodal, with the maximum sub-maximum located in the macropores (capillary pores). Thus, the macropores are also more abundant and the macroporosity is related to other parameters like CWU and weight loss during the salt test.

The kinetics of the CWU are related to the pore radii distribution and total porosity. Stones with a high pore connectivity display a linear absorption of water until they reach the maximum absorption, while stones with low connectivity display an absorption curve with slope breaks. The WVD is directly related to porosity, while the influence of the pore radii size is not so evident.

During the salt crystallization test the stones undergo an increase of porosity with the shift of the pore radii

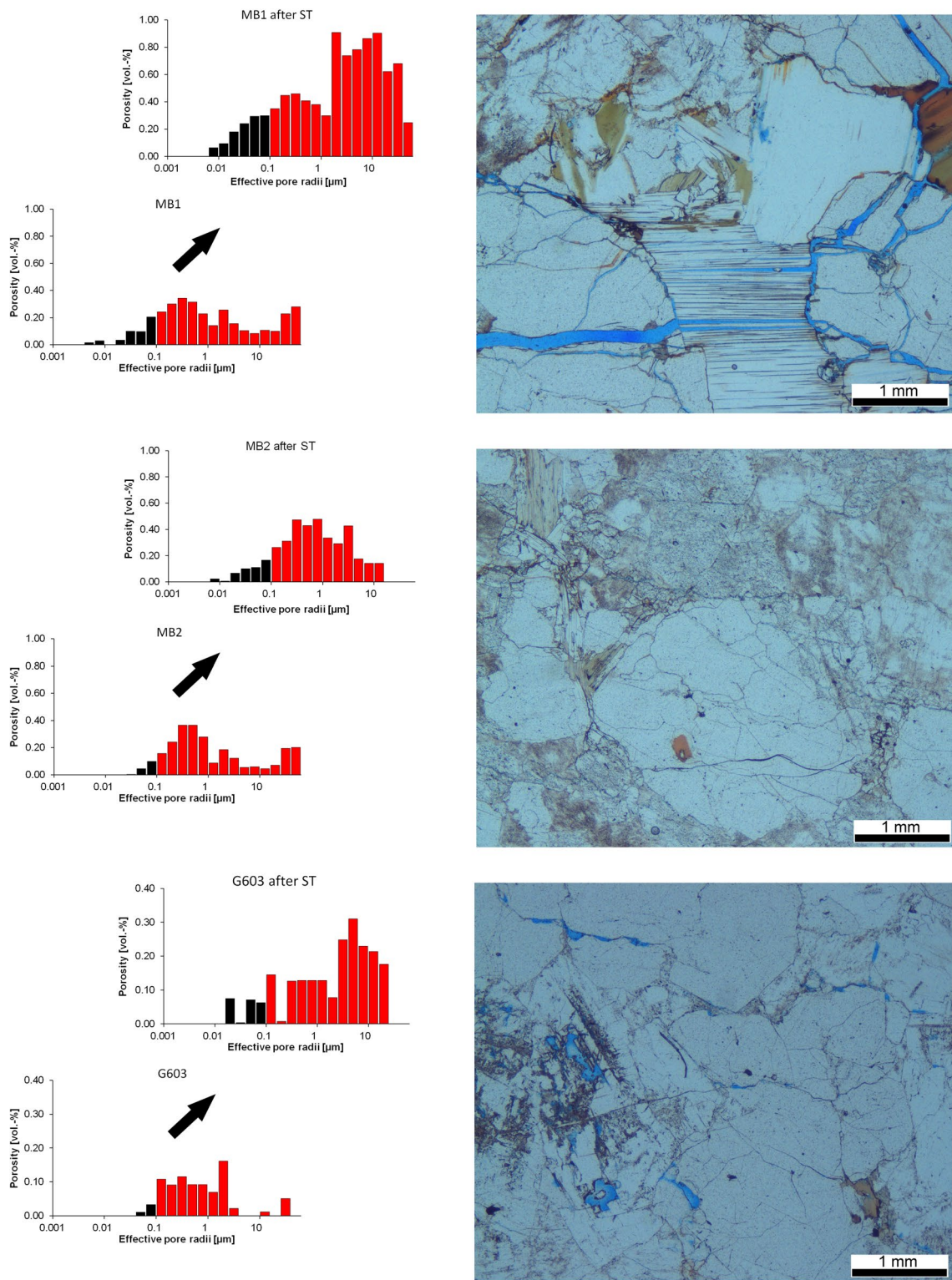


Fig. 25 Examples of the evolution of pore radii distribution and petrographic observations after salt test (from top to bottom: MB1, MB2 and G603)

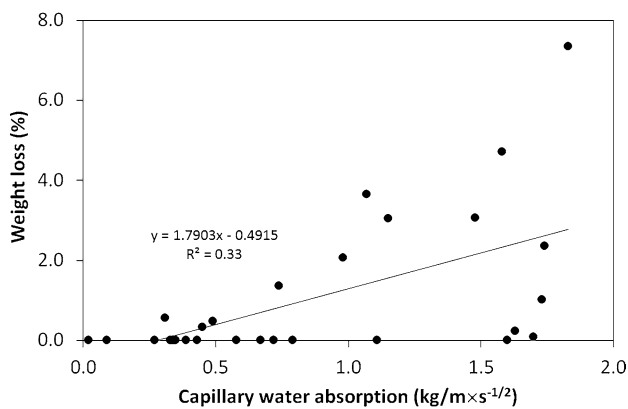


Fig. 26 Relationship between weight variation in crystallization salt test (at 59th cycle) and the capillary water absorption

distribution towards the macropores field. The increase of macropores is a consequence of the propagation and widening of preexistent cracks as well as the development of new ones.

The resistance against salt action, assessed by weight loss during the salt crystallization test, is controlled by the total porosity with some exceptions related to the pore radii size and distribution as well as to the pore connectivity. When the stones have similar porosity, those with a high percentage of macropores will be more prone to lose weight. Stones with high porosity do not suffer the expected salt action if they have a high pore radii size. The yellow granites, more porous than the sound ones, will be more affected by salt action; however, the magnitude of this action is related to the pore radii size.

During the salt crystallization test stones undergo deep changes in the pore network, which are more evident after 100 cycles. The actual standards do not have applicability in such low porous stones and a revision is necessary.

The evolution of granitoids in a more long-term trial should be done to assess the behavior of the less porous stones. Moreover, the influence of different environmental conditions needs to be investigated.

Acknowledgements This work was supported by the DAAD (Az. 57213019) and CRUP (Project A-50/16). The authors gratefully acknowledge Amanda Ricardo and Christopher Pötzl for their help in the laboratory work.

References

Abad SVANK, Tugrul A, Gokceoglu C, Armaghani DJ (2016) Characteristics of weathering zones of granitic rocks in Malaysia for geotechnical engineering design. *Eng Geol* 200:94–103. <https://doi.org/10.1016/j.enggeo.2015.12.006>

- Alonso FJ, Vázquez P, Esbert RM, Ordaz J (2008) Ornamental granite durability: evaluation of damage caused by salt crystallization test. *Mater Constr* 58(289–290):191–201
- Angeli M, Bigas J-P, Benavente D, Menendez B, Hébert R, David C (2007) Salt crystallization in pores: quantification and estimation of damage. *Environ Geol* 52:205–213. <https://doi.org/10.1007/s00254-006-0474-z>
- Anovitz LM, Cole DR (2015) Characterization and analysis of porosity and pore structures. *Rev Mineral Geochem* 80:61–164. <https://doi.org/10.2138/rmg.2015.80.04>
- Arkan F, Ulusay R, Aydın N (2007) Characterization of weathered acidic volcanic rocks and a weathering classification based on a rating system. *Bull Eng Geol Environ* 66:415–430. <https://doi.org/10.1007/s10064-007-0087-0>
- Barbera G, Barone G, Crupi V, Longo F, Maisano G, Majolino D, Mazzoleni P, Raneri S, Teixeira J, Venut V (2014) A multi-technique approach for the determination of the porous structure of building stone. *Eur J Mineral* 26:189–198. <https://doi.org/10.1127/0935-1221/2014/0026-2355>
- Begonha AJS (1997) Meteorização do granito e deterioração da pedra em monumentos e edifícios da cidade do Porto. PhD Thesis, University of Minho
- Begonha A (2009) Mineralogical study of the deterioration of granite stones of two Portuguese churches and characterization of the salt solutions in the porous network by the presence of diatoms. *Mater Charact* 60:621–635. <https://doi.org/10.1016/j.matchar.2008.12.019>
- Benavente D, García del Cura MA, García-Guinea J, Sánchez-Moral S, Ordóñez S (2004a) Role of pore structure in salt crystallisation in unsaturated porous stone. *J Cryst Growth* 260:532–544. <https://doi.org/10.1016/j.jcrysgro.2003.09.004>
- Benavente D, García del Cura MA, Fort R, Sánchez-Moral S, Ordóñez S (2004b) Durability estimation of porous building stones from pore structure and strength. *Eng Geol* 74:113–127. <https://doi.org/10.1016/j.enggeo.2004.03.005>
- Berrezueta E, Kovacs T, Luquot L (2017) Qualitative and quantitative changes of carbonate rocks exposed to SC CO₂ (Basque-Cantabrian Basin, northern Spain). *Appl Sci* 7:1124. <https://doi.org/10.3390/app711124>
- Braga R, Peddis F, Perondi C (2012) Yellowing of a white granite pavement in urban environment: the Fe-rich patina of Piazza Cavalli, Piacenza (Italy). *Periodico Mineral* 81(3):345–357. <https://doi.org/10.2451/2012PM0020>
- Bré JMO (2008) Capela do Senhor da Pedra: Diagnóstico e Proposta de Tratamento da Pedra. Master Thesis, Instituto Superior de Engenharia do Porto
- Buj O, Gisbert J (2010) Influence of pore morphology on the durability of sedimentary building stones from Aragon (Spain) subjected to standard salt decay tests. *Environ Earth Sci* 61:1327–1336. <https://doi.org/10.1007/s12665-010-0451-4>
- Cardell C, Delalieux F, Roumpopoulos K, Moropoulou A, Auger F, Van Grieken R (2003) Salt-induced decay in calcareous stone monuments and buildings in a marine environment in SW France. *Constr Build Mater* 17:165–179
- Caruso F, Flatt RJ (2012) Measuring crystallization pressure: can the Correns' experiment be repeated? In: Proceedings of 12th international congress on the deterioration and conservation of stone. Columbia University, New York
- Çelik MY, Kaçmaz AU (2016) The investigation of static and dynamic capillary by water absorption in porous building stones under normal and salty water conditions. *Environ Earth Sci* 75:307. <https://doi.org/10.1007/s12665-015-5132-x>
- Ceryan S (2015) New weathering indices for evaluating durability and weathering characterization of crystalline rock material: a case study from NE Turkey. *J Afr Earth Sc* 103:54–64. <https://doi.org/10.1016/j.jafrearsci.2014.12.005>

- Coletti C, Cultrone G, Maritana L, Mazzoli C (2016) Combined multi-analytical approach for study of pore system in bricks: how much porosity is there? *Mater Charact* 121:82–92. <https://doi.org/10.1016/j.matchar.2016.09.024>
- Comite V, Álvarez de Buergo M, Barca D, Belfiore CM, Bonazza A, La Russa MF, Pezzino A, Randazzo L, Ruffolo SA (2017) Damage monitoring on carbonate stones: field exposure tests contributing to pollution impact evaluation in two Italian sites. *Constr Build Mater* 152:907–922. <https://doi.org/10.1016/j.conbuildmat.2017.07.048>
- Correns CW, Steinborn W (1939) Experiment zur Messung und Erklärung der sogenannten Kristallisationskraft. *Z Krist* 37:228–238
- Dultz S, Simonyan AV, Pastrana J, Behrens H, Plötze M, Rath T (2013) Implications of pore space characteristics on diffusive transport in basalts and granites. *Environ Earth Sci* 69:969–985. <https://doi.org/10.1007/s12665-012-1981-8>
- Eslami J, Grgic D, Hoxha D (2010) Estimation of the damage of a porous limestone from continuous (P- and S-) wave velocity measurements under uniaxial loading and different hydrous conditions. *Geophys J Int* 183:1362–1375. <https://doi.org/10.1111/j.1365-246X.2010.04801.x>
- Espinosa-Marzal RM, Scherer GW (2008) Crystallization of sodium sulfate salts in limestone. *Environ Geol* 56:605–621. <https://doi.org/10.1007/s00254-008-1441-7>
- Espinosa-Marzal RM, Scherer GW (2013) Impact of in-pore salt crystallization on transport properties. *Environ Earth Sci* 69:2657–2669. <https://doi.org/10.1007/s12665-012-2087-z>
- Espinosa-Marzal RM, Hamilton A, McNall M, Whitaker K, Scherer GW (2011) The chemomechanics of crystallization during rewetting of limestone impregnated with sodium sulfate. *J Mater Res* 26(12):1472–1481. <https://doi.org/10.1557/jmr.2011.137>
- Feijoo J, Nóvoa XR, Rivas T, Mosquera MJ, Taboada J, Montojo C, Carrera F (2013) Granite desalination using electromigration. Influence of type of granite and saline contaminant. *J Cult Heritage* 14:365–376. <https://doi.org/10.1016/j.culher.2012.09.004>
- Feijoo J, Nóvoa XR, Rivas T (2017) Electrokinetic treatment to increase bearing capacity and durability of a granite. *Mater Struct* 50:251. <https://doi.org/10.1617/s11527-017-1123-6>
- Flatt RJ, Mohamed NA, Caruso F, Derluyn H, Desarnaud J, Lubelli B, Espinosa-Marzal RM, Pel L, Rodriguez-Navarro C, Scherer GW, Shahidzadeh N, Steiger M (2017) Predicting salt damage in practice: a theoretical insight into laboratory tests. *RILEM Tech Lett* 2:108–118. <https://doi.org/10.21809/rilemtechlett.2017.41>
- Forestieri G, Freire-Lista DM, Francesco AM, Pontea M, Fort R (2017) Strength anisotropy in building granites. *Int J Architectural Heritage* 11:8. <https://doi.org/10.1080/15583058.2017.1354096>
- Freire-Lista DM, Fort R (2017) Exfoliation microcracks in building granite. Implications for anisotropy. *Eng Geol* 220:85–93. <https://doi.org/10.1016/j.enggeo.2017.01.027>
- Graue B, Siegesmund S, Middendorff B (2011) Quality assessment of replacement stones for the Cologne Cathedral: mineralogical and petrophysical requirements. *Environ Earth Sci* 63:1799–1822. <https://doi.org/10.1007/s12665-011-1077-x>
- Graue B, Siegesmund S, Oyhantcabal P, Naumann R, Licha T, Simon K (2013) The effect of air pollution on stone decay: the decay of the Drachenfels trachyte in industrial, urban, and rural environments—a case study of the Cologne, Altenberg and Xanten Cathedrals. *Environ Earth Sci* 69(4):1095–1124. <https://doi.org/10.1007/s12665-012-2161-6>
- Hirschwald J (1912) *Die Prüfung der natürlichen Bausteine auf ihre Verwitterungsbeständigkeit*. Verlag W Ernest & Sohn, Berlin
- Hosono T, Uchida E, Suda C, Ueno A, Nakagawa T (2006) Salt weathering of sandstone at the Angkor Monuments, Cambodia: identification of the origins of salts using sulfur and strontium isotopes. *J Archaeol Sci* 33:1541–1551. <https://doi.org/10.1016/j.jas.2006.01.018>
- ICOMOS-ISCS (2008) *Illustrated glossary on stone deterioration patterns*. English–French version. ICOMOS Documentation Centre, Paris
- Karagiannis N, Karoglou M, Bakolas A, Moropoulou A (2016) Building materials capillary rise coefficient: concepts, determination and parameters involved. In: Delgado J (ed) *New approaches to building pathology and durability. Building pathology and rehabilitation*, vol 6. Springer, Singapore
- Khanlar GR, Naseri F (2016) Investigation of physical deterioration of Malayer granitic rocks using a new weathering coefficient (Kr4). *Environ Earth Sci* 75:414. <https://doi.org/10.1007/s12665-015-5046-7>
- La Russa MF, Ruffolo SA, Belfiore CM, Aloise P, Randazzo L, Rovella N, Pezzino A, Montana G (2013) Study of the effects of salt crystallization on degradation of limestone rocks. *Periodico Mineral* 82(1):113–127. <https://doi.org/10.2451/2013P M0007>
- La Russa MF, Ruffolo SA, Álvarez de Buergo M, Ricca M, Belfiore CM, Pezzino A, Crisci GM (2017) The behaviour of consolidated Neapolitan yellow Tuff against salt weathering. *Bull Eng Geol Environ* 76:115. <https://doi.org/10.1007/s10064-016-0874-6>
- Laycock EA, Spence K, Jefferson DP, Hetherington S, Martin B, Wood C (2008) Testing the durability of limestone for Cathedral façade restoration. *Environ Geol* 56(3–4):521–528
- Liu Z, Deng D, De Schutter G (2014) Does concrete suffer sulfate salt weathering? *Constr Build Mater* 66:692–701. <https://doi.org/10.1016/j.conbuildmat.2014.06.011>
- López Doncel RA, Wedekind W, Cardona-Velázquez N, González-Sámano PS, Dohrmann R, Siegesmund S, Pötzl C (2016) Geological studies on volcanic tuffs used as natural building stones in the Historical Center of San Luis Potosí, Mexico. In: Hughes JJ, Howind T (eds) *Science and art: a future for stone*. Proceedings of the 13th international congress on the deterioration and conservation of stone, pp 107–105. University of the West of Scotland, Paisley
- López-Arce P, Varas-Muriel MJ, Fernández-Revuelta B, Álvarez de Buergo M, Fort R, Pérez-Soba C (2010) Artificial weathering of Spanish granites subjected to salt crystallization tests: surface roughness quantification. *Catena* 83(2–3):170–185. <https://doi.org/10.1016/j.catena.2010.08.009>
- López-Arce P, Fort R, Gómez-Heras M, Pérez-Monserrat E, Varas-Muriel MJ (2011) Preservation strategies for avoidance of salt crystallisation in El Paular Monastery Cloister, Madrid, Spain. *Environ Earth Sci* 63:1487–1509. <https://doi.org/10.1007/s12665-010-0733-x>
- Ludovico-Marques M, Chastre C (2012) Effect of salt crystallization ageing on the compressive behavior of sandstone blocks in historical buildings. *Eng Fail Anal* 26:247–257. <https://doi.org/10.1016/j.engfailanal.2012.08.001>
- Mielke P, Weinert S, Bignall G, Sass I (2016) Thermo-physical rock properties of greywacke basement rock and intrusive lavas from the Taupo Volcanic Zone, New Zealand. *J Volcanol Geoth Res* 324:179–189. <https://doi.org/10.1016/j.jvolgeores.2016.06.002>
- Molina E, Cultrone G, Sebastián E, Alonso FJ, Carrizo L, Gisbert J, Buj O (2011) The pore system of sedimentary rocks as a key factor in the durability of building materials. *Eng Geol* 118:110–121. <https://doi.org/10.1016/j.enggeo.2011.01.008>
- Molina E, Benavente D, Sebastian E, Cultrone G (2015) The influence of rock fabric in the durability of two sandstones used in the Andalusian Architectural Heritage (Montoro and Ronda, Spain). *Eng Geol* 197:67–81. <https://doi.org/10.1016/j.enggeo.2015.08.009>
- Momeni A, Hashemi SS, Khanlari GR, Heidari M (2017) The effect of weathering on durability and deformability properties of granitoid rocks. *Bull Eng Geol Environ* 76:1037. <https://doi.org/10.1007/s10064-016-0999-7>

- Morales Demarco M, Oyhançabal P, Stein K-J, Siegesmund S (2011) Black dimensional stones: geology, technical properties and deposit characterization of the dolerites from Uruguay. *Environ Earth Sci* 63(7–8):1879–1909. <https://doi.org/10.1007/s12665-010-0827-5>
- Morales Demarco M, Oyhançabal P, Stein K-J, Siegesmund S (2013) Granitic dimensional stones in Uruguay: evaluation and assessment of potential resources. *Environ Earth Sci* 69(4):1397–1438. <https://doi.org/10.1007/s12665-012-2027-y>
- Moreno F, Vilela SAG, Antunes ASG, Alves CAS (2006) Capillary-rising salt pollution and granitic stone erosive decay in the Parish Church of Torre de Moncorvo (NE Portugal)—implications for conservation strategy. *J Cult Heritage* 7:56–66. <https://doi.org/10.1016/j.culher.2005.10.006>
- Mosch S, Siegesmund S (2007) Statistische Bewertung gesteintechnischer Kenndaten von Natursteinen. *Z Dtsch Ges Geowiss* 158(4):821–868
- Mosquera MJ, Rivas T, Prieto B, Silva B (2000) Capillary rise in granitic rocks: interpretation of kinetics on the basis of pore structure. *J Colloid Interface Sci* 222:41–45. <https://doi.org/10.1006/jcis.1999.6612>
- Pazeto AA, Amaral PM, Pinheiro JR, Paraguassú AB (2017) Effects of glass fiber-reinforcement on the mechanical properties of coarse grained building stone. *Constr Build Mater* 155:79–87. <https://doi.org/10.1016/j.conbuildmat.2017.08.063>
- Pérez-Fortes AP, Varas-Muriel MJ, Castiñeiras P (2017) Using petrographic techniques to evaluate the induced effects of NaCl, extreme climatic conditions, and traffic load on Spanish road surfaces. *Mater Constr* 67(328):e138. <https://doi.org/10.3989/mc.2017.07516>
- Prieto B, Silva B (2005) Estimation of the potential bioreceptivity of granitic rocks from their intrinsic properties International. *Bio-deterior Biodegrad* 56:206–215. <https://doi.org/10.1016/j.ibiod.2005.08.001>
- Rivas T, Prieto B, Silva B (2000) Influence of rift and bedding plane on the physico-mechanical properties of granitic rocks. Implications for the deterioration of granitic monuments. *Build Environ* 35:387–396
- Rivas T, Alvarez E, Mosquera MJ, Alejano L, Taboada J (2010) Crystallization modifiers applied in granite desalination: the role of the stone pore structure. *Constr Build Mater* 24:766–776. <https://doi.org/10.1016/j.conbuildmat.2009.10.031>
- Ruedrich J, Siegesmund S (2007) Salt and ice crystallisation in porous sandstones. *Environ Geol* 52(2):225–249
- Saidov TA, Pel L, Kopinga K (2016) Sodium sulfate salt weathering of porous building materials studied by NMR. *Mater Struct* 50:145. <https://doi.org/10.1617/s11527-017-1007-9>
- Sammaljärvi J, Lindberg A, Voutilainen M, Ikonen J, Siitari-Kauppi M, Pitkänen P, Koskinen L (2017) Multi-scale study of the mineral porosity of veined gneiss and pegmatitic granite from Olkiluoto, western Finland. *J Radioanal Nucl Chem* 314(3):1557–1575. <https://doi.org/10.1007/s10967-017-5530-5>
- Schild M, Siegesmund S, Vollbrecht A, Mazurek M (2001) Characterization of granite matrix porosity and pore-space geometry by in situ and laboratory methods. *Geophys J Int* 146(1):111–125
- Siegesmund S, Grimm WD, Dürrast H, Ruedrich J (2010) Limestones in Germany used as building stones: an overview. *Geol Soc Lond Special Publ* 331(1):37–59
- Sousa LMO (2014) Petrophysical properties and durability of granites employed as building stone: a comprehensive evaluation. *Bull Eng Geol Environ* 73(2):569–588. <https://doi.org/10.1007/s10064-013-0553-9>
- Sousa L, Barabasz J, Stein K-J, Siegesmund S (2017) Characterization and quality assessment of granitic building stone deposits: a case study of two different Portuguese granites. *Eng Geol* 221:29–40. <https://doi.org/10.1016/j.enggeo.2017.01.030>
- Streckeisen A (1976) To each plutonic rock its proper name. *Earth Sci Rev* 12(1):1–33
- Stück H, Plagge R, Siegesmund S (2013) Numerical modeling of moisture transport in sandstone: the influence of pore space, fabric and clay content. *Environ Earth Sci* 69(4):1161–1187. <https://doi.org/10.1007/s12665-013-2405-0>
- Theoulakis P, Moropoulou A (1997) Microstructural and mechanical parameters determining the susceptibility of porous building stones to salt decay. *Constr Build Mater* 11(1):65–71
- Thomachot-Schneider C, Gommeaux M, Fronteau G (2008) Modifications of the porous network of sandstone accompanying the formation of black varnish. *Environ Geol* 56:571–582. <https://doi.org/10.1007/s00254-008-1443-5>
- Thomachot-Schneider C, Gommeaux M, Lelarge N, Conreux A, Mouhoubi K, Bodnar J-L, Vázquez P (2016) Relationship between Na₂SO₄ concentration and thermal response of reconstituted stone in the laboratory and on site. *Environ Earth Sci* 75:762. <https://doi.org/10.1007/s12665-016-5388-9>
- Torkan M, Irannezhadi MR, Baghbanan AR (2016) Alteration dependent physical–mechanical properties of quartz-diorite building stones. *Int J Min Geoeng* 50(2):195–200. <https://doi.org/10.22059/ijmge.2016.59829>
- Török A, Czinder B (2017) Relationship between density, compressive strength, tensile strength and aggregate properties of andesites from Hungary. *Environ Earth Sci* 76:639. <https://doi.org/10.1007/s12665-017-6977-y>
- Tuğrul A (2004) The effect of weathering on pore geometry and compressive strength of selected rock types from Turkey. *Eng Geol* 75:215–227. <https://doi.org/10.1016/j.enggeo.2004.05.008>
- Tullborg EL, Larson SA (2006) Porosity in crystalline rocks—a matter of scale. *Eng Geol* 84:75–83
- Unterwurzacher M, Mirwald PW (2008) Initial stages of carbonate weathering: climate chamber studies under realistic pollution conditions. *Environ Geol* 56:507–519. <https://doi.org/10.1007/s00254-008-1440-8>
- Lubelli B, van Hees RPI, Nijland TG (2014) Salt crystallization damage: how realistic are existing ageing tests? In van Breugel K, Koenders EAB (eds) Proceedings of the international conference on ageing of materials and structures, Delft, pp 103–111
- Vázquez P, Alonso FJ, Esbert RM, Ordaz J (2010) Ornamental granites: relationships between p-waves velocity, water capillary absorption and the crack network. *Constr Build Mater* 24:2536–2541. <https://doi.org/10.1016/j.conbuildmat.2010.06.002>
- Vázquez P, Luque A, Alonso FJ, Grossi CM (2013) Surface changes on crystalline stones due to salt crystallisation. *Environ Earth Sci* 69(4):1237–1248. <https://doi.org/10.1007/s12665-012-2003-6>
- Vázquez P, Acuña M, Benavente D, Gibeaux S, Navarro I, Gomez-Heras M (2016) Evolution of surface properties of ornamental granitoids exposed to high temperatures. *Constr Build Mater* 104:263–275. <https://doi.org/10.1016/j.conbuildmat.2015.12.051>
- Vázquez-Nion D, Silva B, Prieto B (2018) Influence of the properties of granitic rocks on their bioreceptivity to subaerial phototrophic biofilms. *Sci Total Environ* 610–611:44–54. <https://doi.org/10.1016/j.scitotenv.2017.08.015>
- Viles HA (2013) Durability and conservation of stone: coping with complexity. *Q J Eng Geol Hydrogeol* 46:367–375. <https://doi.org/10.1144/qjagh2012-053>
- von Moss A, De Quervain F (1948) *Technische Gesteinskunde*. Birkhäuser, Basel
- Warke PA, Smith BJ, Lehane E (2011) Micro-environmental change as a trigger for granite decay in offshore Irish lighthouses: implications for the long-term preservation of operational historic buildings. *Environ Earth Sci* 63:1415–1431. <https://doi.org/10.1007/s12665-010-0662-8>
- Wedekind W, López-Doncel R, Dohrmann R, Kocher M, Siegesmund S (2013) Weathering of volcanic tuff rocks caused by

- moisture expansion. *Environ Earth Sci* 69:1203–1224. <https://doi.org/10.1007/s12665-012-2158-1>
- Wilhelm K, Viles H, Burke Ö (2016) The influence of salt on handheld electrical moisture meters: can they be used to detect salt problems in porous stone? *Int J Architectural Heritage* 10(6):735–748. <https://doi.org/10.1080/15583058.2015.1109733>
- Winkler EM (1973) *Stone: properties, durability in man's environment*. Springer, Berlin
- Yu S, Oguchi CT (2010) Role of pore size distribution in salt uptake, damage, and predicting salt susceptibility of eight types of Japanese building stones. *Eng Geol* 115:226–236. <https://doi.org/10.1016/j.enggeo.2009.05.007>
- Zedef V, Unal M (2010) Effect of salt crystallization on the building stones used in Konya, central Turkey. *Int J Econ Environ Geol* 1(1):51–52
- Sawdy-Heritage AM, Heritage A, Pel L (2008) A review of salt transport in porous media: assessment methods and salt reduction treatments. In *Salt weathering on buildings and stone sculptures (SWBSS)*, 22–24 October 2008, Copenhagen, Denmark
- Leite ALFC (2008) Estudo da deterioração da pedra na Igreja de Santa Clara em Vila do Conde. Master Thesis, Engineering Faculty, University of Porto
- Klopfner H (1985) Feuchte. In: Lutz et al (eds) *Lehrbuch der Bauphysik*. Teubner, Stuttgart
- Jamshidi A, Zamanian H, Sahamieh RZ (in press) The effect of density and porosity on the correlation between uniaxial compressive strength and P-wave velocity. *Rock Mech Rock Eng* (accepted). <https://doi.org/10.1007/s00603-0171379-8>
- Vázquez P, Esbert RM, Alonso FJ, et Ordaz J (2008) Evaluation of damage induced by salt crystallization in granitic building stones. In: 11th International congress on deterioration and conservation of Stone Torún, vol I, pp 325–331
- Hoffmann A (2007) *Naturwerksteine Thailand: Lagerstättenerkundung und Bewertung*. <http://webdoc.sub.gwdg.de/diss/2007/hoffmann/hoffmann.pdf>. Accessed 19 Dec 2017
- Henriques AME, Tello JSMN (2006) *Manual da pedra natural para a arquitetura*. Direcção Geral da Geologia e Energia. ISBN 989-95163-0-9
- Fojo ACOT (2006) Estudo da aplicação de consolidantes e hidrófugos em pedras graníticas da Igreja Matriz de Caminha. Master Thesis, Engineering Faculty, University of Porto
- Ferreira JMLC (2011) Degradação da pedra provocada por sais em edifícios antigos. Master Thesis, Engineering Faculty, University of Porto
- Vicente MA (1996) Final report 1991–1994—Project STEP-CT-0101—granitic materials and historical monuments: study of the factors and mechanisms of weathering and application to historical heritage conservation. In: Vicente MA, Rodrigues JD, Acevedo J (eds) *Proceedings of the European Commission workshop degradation and conservation of granitic rocks in monuments, Santiago de Compostela*. Protection and conservation of European cultural heritage, research report n° 5, pp 1–44
- Espinosa-Marzal RM, Scherer GW (2010) Mechanisms of damage by salt. *Geological Society, London, Special Publications*, vol 331, pp 61–77. <https://doi.org/10.1144/SP331.5>
- Doehne E (2002) Salt weathering: a selective review. In: Siegesmund S, Weiss T, Vollbrecht A (eds) *Natural stone, weathering phenomena, conservation strategies and case studies*. Geological Society of London, Special Publications vol 205, pp 51–64
- Begonha A, Jeannette D, Hammecker C, Braga MAS (1994) Physical characteristics of the Oporto granite related to stone decay in monuments. In: Fassina V, Ott H, Zezza F (eds) *Proc. 3° Simposio Internazionale La Conservazione dei Monumenti nel Bacino del Mediterraneo – Venezia*, pp 541–546
- Barroso CE, Oliveira DV, Ramos LF (in press) Vernacular schist farm walls: materials, construction techniques and sustainable rebuilding solutions. *J Build Eng* (accepted). <https://doi.org/10.1016/j.jobe.2017.12.001>
- Antão A, Quinta-Ferreira M (2015) Weathering influence on physical properties of the Guarda granite, Portugal. In: *Proceedings of the 15th international SGEM geoconference on science and technologies in geology, exploration and mining*. <https://doi.org/10.5593/SGEM2015/B12/S2.115>
- Alencar CRA (2013) *Manual de caracterização, aplicação, uso e manutenção das principais rochas comerciais no Espírito Santo: rochas ornamentais*. Instituto Euvaldo Lodi - Regional do Espírito Santo, Cachoeiro de Itapemirim
- LNEC (1990a) Estudos relativos à alteração e conservação do granito do claustro do Mosteiro de Grijó, em Vila Nova de Gaia. Relatório 243/90-GERO/NQ, Lisboa
- Ruedrich J, Sigismund S (2006) Fabric dependence of length change behaviour induced by ice crystallization in the pore space of natural building stones. In: Fort A, Alvarez de Buergo M, Gomez-Heras M et al (eds) *Heritage, weathering and conservation*. Taylor and Francis Group, London
- LNEC (1990b) Estudo relativo à acção dos pombos sobre a pedra das igrejas do Carmo e dos Carmelitas, no Porto, e de São Gonçalo, em Amarante. Relatório 243/9-GERO/NQ, Lisboa
- Martins ML, Vasconcelos G, Lourenço PB, Palha C (2016) Influence of the salt crystallization in the durability of granites used in vernacular masonry buildings. In: Modena C, da Porto F, Valluzzi MR (eds) *Brick and block masonry—trends, innovations and challenges*. Taylor and Francis Group, London, pp 517–524. ISBN 978-1-138-02999-6
- Ribeiro CMM (2013) Avaliação do desempenho de revestimentos superficiais na durabilidade de pedra de construção. Master Thesis, Engineering Scholl, University of Minho
- Sengun N, Demirdag S, Akbay D, Ugur I, Altindag R, Akbulut A (2014) Investigation of the relationships between capillary water absorption coefficients and other rock properties of some natural stones, V. In: *Global stone congress, 22–25 October 2014, Antalya/Türkiye*
- Shahidzadeh N, Desarnaud J, Bonn D (2016) Direct measurement of salt crystallization pressure at the pore scale. In: Hughes J, Howind T (eds) *Science and art: a future for stone: proceedings of the 13th international congress on the deterioration and conservation of stone, vol 1*. University of the West of Scotland, Paisley, pp 467–474
- Siedel H, Siegesmund S (2014) Characterization of stone deterioration on buildings. In: Siegesmund S, Snehlage R (eds) *Stone in architecture. Properties, durability*, 5th edn. Springer
- Siegesmund S, Dürrast H (2014) Physical and mechanical properties of the rocks. In: Siegesmund S, Snehlage R (eds) *Stone in architecture. Properties, durability*, 5th edn. Springer
- Poschold K (1990) *Das Wasser im Porenraum kristalliner Naturwerksteine und sein Einfluß auf die Verwitterung*. Münchner Geowissenschaftliche Abhandlungen Reihe B Allgemeine und Angewandte Geologie
- Silva AC (2012) Estudo diagnóstico, cartografia e proposta de tratamento das deteriorações do granito do Hospital da Santa Casa da Misericórdia de Viana do Castelo. Master Thesis, Engineering Faculty, University of Porto
- Pinto APF, Rodrigues JD, Costa DR (1994) Assessment of the efficacy and harmfulness of water repellents in granite. In: Fassina V, Ott H, Zezza F (eds) *Proc. 3° Simposio Internazionale La Conservazione dei Monumenti nel Bacino del Mediterraneo, Venezia*, pp 883–889
- Pérez-Ortiz A, Ordaz J, Esbert RM, Alonso FJ, Días-Pache F (1996) Physical behaviour degradation trends in an anisotropic granite. In: Riederer J (ed) *Proceedings of the 8th international congress on deterioration and conservation of stone, Berlin*, pp 205–209

- Steiger M, Charola AE, Sterflinger K (2014) Weathering and deterioration. In: Siegesmund S, Snethlage R (eds) *Stone in architecture. Properties, durability*, 5th edn. Springer
- Mosch S (2009) *Optimierung der Exploration, Gewinnung und Materialcharakterisierung von Naturwerksteinen*. <http://webdoc.sub.gwdg.de/diss/2009/mosch/mosch.pdf>. Accessed 19 Dec 2017
- Strohmeier D (2003) *Gefügeabhängigkeit technischer Gesteinseigenschaften*. Dissertation zur Erlangung des Doktorgrades Mathematisch-Naturwissenschaftliche Fakultäten der Georg-August-Universität zu Göttingen
- Stu E, Eggers T, Cassar J, Ruedrich J, Fitzner B, Siegesmund S (2007) Stone properties and weathering induced by salt crystallization of Maltese Globigerina Limestone. In: Přikryl R, Smith BJ (eds) *Building stone decay: from diagnosis to conservation*. Geological Society, London, Special Publications 271:189–198
- Morales Demarco M (2012) *Mineralogical, petrophysical and economical characterization of the dimensional stones of Uruguay; implications for deposit exploration*. PhD Thesis, University of Gottingen
- Mendes PIP (2013) *Estudos sobre a Igreja de São Domingos em Viana do Castelo: bases para intervenção de conservação exterior*. Master Thesis, University of Trás-os-Montes e Alto Douro
- LNEC (1990c) *Estudo relativo à alteração e conservação do granito da Torre dos Clérigos, no Porto*. Relatório 243/9-GERO/NQ, Lisboa
- MacWilliam K (2017) *Aging tests to assess the durability of building materials to salt crystallization—towards a more realistic and effective use of sodium sulfate*. MSc Dissertation, Czech Technical University, Prague